



# New insights into the primary production and the structure of the phytoplankton community in the South Indian Ocean using size fractionation experiments

Valentin Deteix<sup>1</sup>, Céline Ridame<sup>1</sup>, Céline Dimier<sup>2</sup>, Claire Lo Monaco<sup>1</sup>, Aline Tribollet<sup>1</sup>, Frédéric Planchon<sup>3</sup>

<sup>1</sup> LOCEAN-IPSL, Laboratoire d'Océanographie et du Climat : Expérimentations et Approches Numériques, UMR 7159 (Sorbonne Université-CNRS-MNHN-IRD), 4 Place Jussieu, 75005 Paris, France

<sup>2</sup> IMEV, Institut de la Mer de Villefranche, FR 3761 (Sorbonne Université, CNRS), 181 Chemin du Lazaret, 06230 Villefranche-sur-Mer, France

<sup>3</sup> LEMAR, Laboratoire des Sciences de l'Environnement Marin, UMR 6539 (Univ. Brest-CNRS-IRD-Ifremer), Institut Universitaire Européen de la Mer, F-29280 Plouzané, France

Correspondence to: Valentin Deteix ([valentin.deteix@locean.ipsl.fr](mailto:valentin.deteix@locean.ipsl.fr)); Céline Ridame ([celine.ridame@locean.ipsl.fr](mailto:celine.ridame@locean.ipsl.fr))

**Abstract.** As part of the South Indian Ocean CARBOn fluxes from the surface to the mesopelagic twilight zone (SOCARB) project, the phytoplankton biomass and net primary production (NPP), along with the biomass of phytoplankton chemotaxonomic groups, were assessed in contrasting biogeochemical areas of the South Indian and Southern Oceans in late austral summer 2023. A size fractionation approach was performed to characterize the size structure of primary production and phytoplankton chemotaxonomic groups biomass in three size classes: picophytoplankton ( $< 3 \mu\text{m}$ ), nanophytoplankton ( $3\text{--}20 \mu\text{m}$ ), and microphytoplankton ( $> 20 \mu\text{m}$ ). Across the study area, NPP was dominated by microphytoplankton ( $56\% \pm 21\%$ ) while total chlorophyll *a* (TChl*a*) was sustained by nano- ( $40\% \pm 11\%$ ) and microphytoplankton ( $37\% \pm 18\%$ ), notably by nanophytoplankton haptophytes and microphytoplankton diatoms. Our results highlighted the spatial variability of NPP and TChl*a* size structures, mainly driven by temperature, salinity and macronutrients – mainly N, P. In the Subtropical and Subantarctic zones, NPP and TChl*a* were sustained by pico- and nanophytoplankton with a diversified community (cyanobacteria, haptophytes, chlorophytes, pelagophytes). Conversely in the Polar Frontal and Antarctic zones, NPP and TChl*a* were dominated by nano- and microphytoplankton with a less diversified community (diatoms, haptophytes). Our results also underline the intra-zonal variability of NPP and TChl*a* through bottom-up processes, such as cyclonic eddy in the Subtropical zone or Si-depleted water mass intrusion in the Polar Frontal zone. Focusing on the links between NPP and TChl*a* size structure across the study area, NPP was mainly driven by the biomass of nano- and microphytoplankton, more specifically by the biomass of nano- and microphytoplankton diatoms, haptophytes and dinoflagellates. This study paves the way for a better understanding of phytoplankton productivity and community size structure, which could contribute to a more detailed knowledge on their role in the biological carbon pump.



## 1 Introduction

One of the main challenges in marine biogeochemistry is to understand the impact of factors controlling the efficiency of the soft tissue pump, or so-called “biological carbon pump” (BCP). Among these factors, the intensity of net primary production (NPP) and the structure of phytoplankton communities are known to play key roles in biogeochemical fluxes involved in the BCP and depend on the chemico-physical conditions of the ocean. More specifically, the taxonomic composition and the size structure of phytoplankton communities can affect significantly the intensity and fate of NPP by controlling the photosynthetic CO<sub>2</sub> uptake efficiency (*e.g.* Cermeño et al., 2005), the transfer of NPP through either microbial trophic pathway or higher trophic levels (*e.g.* Marañón, 2009) and the carbon export and sequestration in the deep ocean (*e.g.* Guidi et al., 2009). Therefore, considering phytoplankton as a single generic variable is irrelevant for fully understanding the BCP. To tackle this issue, a common approach is to assess phytoplankton in size classes, either through size fractionation experiments to quantify size structure and its associated fluxes such as NPP (*e.g.* Froneman et al., 2001; Marañón et al., 2001) or from phytoplankton functional type approaches used to estimate phytoplankton size structure from bulk measurements (*e.g.* Uitz et al., 2006; Hirata et al., 2011).

The South Indian Ocean (SIO), including the Indian sector of the Southern Ocean, is a unique oceanic region with contrasting biogeochemical features. Since the first monitoring measurements of air-sea CO<sub>2</sub> fluxes in this region carried out by Metzl et al. (1995), the Southern Ocean, south of the Subtropical Front (STF), is known to be a net CO<sub>2</sub> sink (Takahashi et al., 2009; Hauck et al., 2023). It is characterized by High Nutrient Low Chlorophyll (HNLC) conditions, with low phytoplankton biomass (< 0.5 mg m<sup>-3</sup>) despite high macronutrients concentrations (NO<sub>x</sub> (NO<sub>3</sub><sup>-</sup> + NO<sub>2</sub><sup>-</sup>), dissolved inorganic phosphorus (DIP)). This paradox is explained by limitations of the phytoplankton growth by micronutrients, especially iron (Fe) (Martin, 1990; Martin et al., 1990) or manganese (Mn) (Browning et al., 2021; Hawco et al., 2022) and by secondary limiting factors such as light, water column stability and grazing pressure (Moore and Abbott, 2000). Furthermore, the Southern Ocean is characterized by the Antarctic Circumpolar Current (ACC), a massive eastward flowing current driven by westerly winds, that divides the region into several hydrographic zones defined by specific water masses and fronts (Nowlin and Klinck, 1986). The Antarctic Zone (AZ), south of the Polar Front (PF), exhibits typical HNLC conditions (Minas and Minas, 1992). The Polar Frontal Zone (PFZ), between the PF and the Subantarctic Front (SAF), and the Subantarctic Zone (SAZ), between the SAF and the STF, display high NO<sub>x</sub> and DIP concentrations but low dissolved silicon (DSi) concentrations (usually < 5 μmol L<sup>-1</sup>), resulting in High Nutrient Low Silicon Low Chlorophyll (HN-LSi-LC) conditions (Nelson et al., 2001; Sarmiento et al., 2004). The STF delineates the boundary between the Southern Ocean and the Subtropical Zone (STZ) of the SIO, which is characterized by Low Nutrient Low Chlorophyll (LNLC) conditions (McClain et al., 2004) and acts as a CO<sub>2</sub> source during austral summer (Sarma et al., 2023).

While the contrasting physical and biogeochemical regimes in the SIO exert strong bottom-up control on phytoplankton biomass, composition and productivity (Hörstmann et al., 2021; Hayward et al., 2024), most of this knowledge is restricted to the upper surface layer. By contrast, much less is known about these phytoplankton characteristics within the



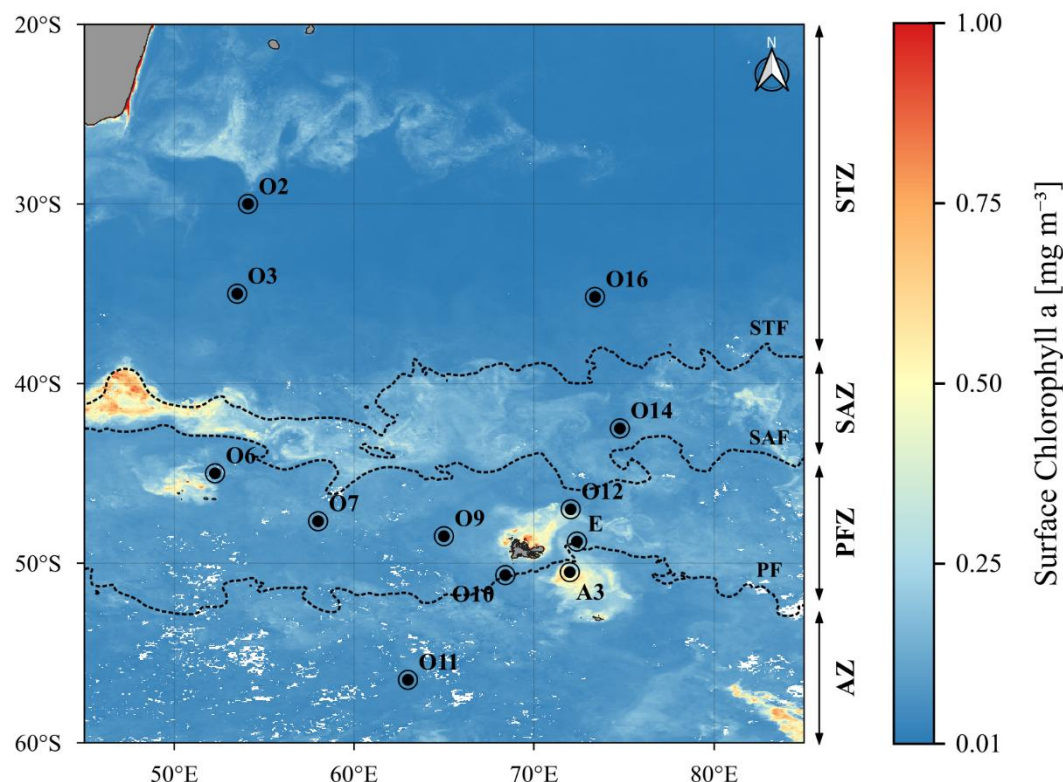
65 euphotic layer, especially as these features were mostly determined from bulk measurements. Moreover, previous field studies  
 conducted in the SIO investigating phytoplankton composition and size structure within the euphotic layer have primarily  
 focused on high productivity regions – *i.e.* areas in the vicinity of subantarctic islands – where enhanced surface NPP results  
 from natural Fe fertilization (Blain et al., 2007; Pollard et al., 2009; Holmes et al., 2020) such as Crozet Islands (Seeyave et  
 al., 2007), Kerguelen Islands (Uitz et al., 2009; Lasbleiz et al., 2014; Cavagna et al., 2015), Heard and McDonald Islands  
 70 (Wojtasiewicz et al., 2019). By contrast, the vast low productivity regions of the SIO with LNLC, HN-LSi-LC and HNLC  
 conditions have received considerably less attention, despite covering the majority of the SIO. While some studies have  
 provided relevant insights into phytoplankton biomass and composition in the upper water column using pigment  
 chemotaxonomy tools (Schlüter et al., 2011; Mendes et al., 2015; Latasa et al., 2023), data remain scarce, particularly  
 concerning NPP (Leblanc et al., 2002; Jasmine et al., 2009; Gandhi et al., 2012).

75 The SOCARB (South Indian Ocean CARBon fluxes from the surface to the mesopelagic twilight zone) cruise took  
 place during the late austral summer of 2023. SOCARB aims to provide key metrics to characterize the BCP components and  
 the associated fluxes of organic carbon, from the euphotic layer to the base of the mesopelagic zone in the SIO. SOCARB was  
 implemented as part of the long-term monitoring program OISO (Océan Indien Service d'Observations), involved since 1998  
 in the long-term monitoring of oceanic CO<sub>2</sub> parameters in the SIO. This opportunity allowed us to investigate phytoplankton  
 80 NPP, biomass and community size structure, along with their respective size structures across contrasting biogeochemical  
 regions of the SIO. The first objective was to describe the size structure (pico-, nano- and microphytoplankton) of (i) the net  
 primary production, (ii) the phytoplankton biomass (total chlorophyll *a*) and (iii) the biomass of phytoplankton  
 chemotaxonomic groups. The second objective was to assess their vertical and spatial variability in relation to the  
 environmental conditions. The third objective was to determine whether NPP is determined by the size structure of the  
 85 phytoplankton biomass and/or by the size structure of the biomass of specific phytoplankton chemotaxonomic groups.

## 2 Materials and Methods

### 2.1 Cruise transect – Sampling Strategy

Our study was part of the MD240 / OISO33-SOCARB cruise (Lo Monaco et al., 2023) on board the R/V *Marion*  
*Dufresne II*, conducted in the South Indian and Southern Oceans during austral summer, from January 23<sup>rd</sup> to February 28<sup>th</sup>,  
 90 2023. SOCARB experiments were conducted at twelve stations in contrasting biogeochemical regions (Fig. 1), including the  
 oligotrophic subtropical gyre of the SIO characterised by LNLC conditions, open ocean regions exhibiting HNLC or HN-LSi-  
 LC characteristics, and bloom areas near Subantarctic islands such as the Crozet Islands and Kerguelen Plateau, both renowned  
 for being naturally iron-fertilized regions (Blain et al., 2007; Pollard et al., 2009).



95 **Figure 1: Map of the OISO33-SOCARB study area showing the location of the stations from this study, overlying the satellite-**  
**derived surface chlorophyll *a* concentration averaged over February 2023 (MODIS L3 product). The dotted lines indicate the**  
**positions of the main fronts determined from satellite-derived surface temperature averaged over February 2023 (CMEMS L4**  
**product): STF, Subtropical Front (18°C); SAF, Subantarctic Front (13°C); PF, Polar Front (4.5°C).**

Seawater was collected using a CTD (Sea-Bird SBE 911 Plus) mounted on a rosette equipped with 24 Niskin bottles  
 100 (12 L, General Oceanics, Inc.). Samples for phytoplankton primary production and pigments were collected at six depths,  
 between the surface (~ 10 m) and 200 m maximum. Sampling depths were determined from the fluorescence downcast profiles  
 during the CTD measurements acquisition, to best describe the fluorescence profile and its gradients, such as subsurface  
 chlorophyll maximum (SCM).

## 2.2 Size fractionated primary production

105 All materials were acid-washed (HCl Suprapur 32%) following trace metal clean procedures (Cutter et al., 2017), and  
 polycarbonate bottles were rinsed three times before sampling with the collected seawater. For NPP, 2.3 L of unfiltered  
 seawater was collected for the total fraction and 5.5 L for the size fractions. Prefiltration was performed using 20 and 3  $\mu\text{m}$   
 filter cartridge (Sartorius) under pressurised filtration units. For each prefiltration, bottles were rinsed three times with the  
 seawater filtrates, and 2.3 L of respectively < 20  $\mu\text{m}$  and < 3  $\mu\text{m}$  seawater filtrates were collected. This size fractionation



110 approach enabled us to determine the contributions of the three phytoplankton size classes: picophytoplankton ( $< 3 \mu\text{m}$ ),  
 nanophytoplankton ( $3\text{--}20 \mu\text{m}$ ), and microphytoplankton ( $> 20 \mu\text{m}$ ) (Sieburth et al., 1978; Vaulot et al., 2008). NPP rates were  
 determined using the  $^{13}\text{C}$  tracer addition method (Hama et al., 1983; Ridame et al., 2022) in the total,  $< 20 \mu\text{m}$  and  $< 3 \mu\text{m}$   
 fractions. After prefiltration, 1 mL of  $\text{NaH}^{13}\text{CO}_3$  (99%; Eurisotop) was added to the bottles to obtain a final  $^{13}\text{C}$  enrichment of  
 ~ 10%. Each bottle was shaken vigorously before incubation for 24 h in on-deck containers with circulating seawater. To  
 115 simulate an irradiance level as close as possible to the sampled depth, blue filters with several sets of blue neutral density filters  
 were used (LEE Filters: 75, 54.4, 36, 19.3, 10.4, 5.6, 2.7 and 1% attenuation). After 24 h incubation, 2.3 L was vacuum filtered  
 ( $< 200 \text{ mbar}$ ) onto pre-combusted ( $450^\circ\text{C}$ ) 25 mm GF/F filters (Whatman<sup>TM</sup> glass microfiber) and stored at  $-20^\circ\text{C}$ . Filters  
 were dried at  $40^\circ\text{C}$  for 48 h before analysis at the Alysés analytical platform (IRD-SU, Bondy, France). In addition, 2.3 L of  
 surface and SCM seawaters were immediately filtered after collection onto pre-combusted GF/F filters to determine natural  
 120 concentration and isotopic signature of particulate organic carbon (POC). POC and  $^{13}\text{C}$  isotopic ratio were quantified using an  
 online continuous flow elemental analyser (EA, Thermo Fisher Scientific Inc. Flash 2000 HT) coupled with an isotopic ratio  
 mass spectrometer (IRMS, Thermo Fisher Scientific Inc. Delta V Advantage via a ConFlow IV interface). For each sample,  
 POC was higher than the experimental detection limit of  $0.42 \mu\text{mol C}$ , defined as three times the standard deviation of the  
 blanks. The mean natural  $^{13}\text{C}$  signature was  $1.081 \pm 0.002 \text{ atom\%}$  ( $n = 24$ ), with no significant differences between surface  
 and SCM values (Student test:  $t = -0.1491$ ,  $p = 0.88$ ). The atom% excess of the dissolved inorganic carbon (DIC) was calculated  
 125 by using DIC concentrations measured at the SNAPO- $\text{CO}_2$  analytical platform (LOCEAN-IPSL, Paris, France, Metzl et al.,  
 2025).

### 2.3 Size fractionated phytoplankton pigments

The size fractionation filtration procedure was the same as described for the NPP (see section 2.2). For pigments, 2.3  
 130 L of unfiltered seawater was directly filtered onto GF/F filters for the total fraction, and 3.5 L of  $< 20 \mu\text{m}$  and  $< 3 \mu\text{m}$  seawater  
 filtrates were filtered onto GF/F filters. The filters were placed in cryotubes, flash-frozen in liquid nitrogen and stored at  $-80^\circ\text{C}$   
 until analysis at the SAPIGH analytical platform (IMEV, Villefranche-sur-Mer, France). Filters were extracted during 2  
 hours in 3 mL HPLC-grade methanol (100%) containing an internal standard (Vitamin E acetate, Sigma), sonicated once and  
 then clarified by vacuum filtration through GF/F filters. Extracts analysis was carried out within 24 h after extraction using an  
 135 Agilent Technologies Inc. 1200 series HPLC system. The general procedure for HPLC pigment analysis, identification and  
 quantification is described in Ras et al. (2008). This method allows the detection of 26 separate pigments with low detection  
 limits ( $\leq 0.0002 \text{ mg m}^{-3}$ ). Pigments include chlorophyll *a* (Chla) and divinyl-chlorophyll *a* (DVChla), whose sum of the  
 concentrations is referred to as total chlorophyll *a* (TChla), an indicator of the phytoplankton biomass. Pigments also include  
 various accessory pigments, some of which can be used as biomarkers of phytoplankton taxonomic groups (Higgins et al.,  
 140 2011). In this study, the following eleven accessory pigments were further used to study the TChla biomass of the  
 phytoplankton chemotaxonomic groups: fucoxanthin (Fuco), peridinin (Peri), 19'-hexanoyloxyfucoxanthin (Hex-fuco), 19'-



butanoyloxyfucoxanthin (But-fuco), alloxanthin (Allo), chlorophyll *b* (Chl*b*), zeaxanthin (Zea), neoxanthin (Neo), prasinoxanthin (Pras), violaxanthin (Viola) and DVChl*a*.

## 2.4 Biomass of the phytoplankton chemotaxonomic groups

145 To estimate the Chl*a* biomass of different phytoplankton chemotaxonomic groups from pigment concentrations measured in the sizes classes, we used the open-source R package *phytclass* (v.2.0.0; <https://cran.r-project.org/package=phytclass>), following the procedure described in Hayward et al. (2023). Compared to the commonly used CHEMTAX algorithm (Mackey et al., 1996), the *phytclass* algorithm improves the accuracy of the phytoplankton group biomass estimates, and removes the need for initial assumptions about their pigment:Chl*a* ratios (Hayward et al., 2023).  
 150 Briefly, datasets were first clustered based on their pigment:Chl*a* ratios, then loaded into *phytclass* set with an iteration of 500, a step of 0.009 and 7 phytoplankton chemotaxonomic groups: diatoms, haptophytes, cryptophytes, dinoflagellates, chlorophytes, pelagophytes and *Synechococcus*. After *phytclass* analyses, an 8<sup>th</sup> taxonomic group, *Prochlorococcus*, was added by using DVChl*a*, which was summed with Chl*a* to obtain the TChl*a* biomass of phytoplankton community.

## 2.5 Ancillary supporting data

155 The depth of the surface mixed layer ( $Z_{SML}$ ), defined as the depth at which the density anomaly ( $\sigma$ , kg m<sup>-3</sup>) differed by 0.03 kg m<sup>-3</sup> from the 10 m  $\sigma$  value (de Boyer Montégut et al., 2004), was determined from the CTD downcast profiles. The depth of the euphotic layer ( $Z_{EL}$ ) was determined from the downcast profiles of photosynthetically active radiation (PAR, 400-700 nm, Biospherical Instruments Inc. QCP 2350) and from the surface reference measurements (Biospherical Instruments Inc. QCR 2200). Here, we defined two  $Z_{EL}$ :  $Z_{EL1\%}$  corresponding to the depth at which PAR is reduced to 1% of its surface value (Morel and Berthon, 1989), and  $Z_{EL0.01\%}$  representing the depth at which PAR is reduced to 0.01% of its surface value.  
 160  $Z_{EL0.01\%}$  was subsequently used for the integration of biogeochemical parameters (see section 2.6 and text S1).

Macronutrients samples were collected at fixed depths, and bottles were rinsed three times before sampling with the collected seawater. 30 mL of seawater were filtered through 0.4  $\mu$ m filters and poisoned with 100  $\mu$ L saturated HgCl<sub>2</sub> to stop biological activity, and stored at 4 °C until analysis at the IMAGO analytical platform (IRD, Plouzané, France). NO<sub>x</sub>, DIP and  
 165 DSi were analysed by colorimetry using a segmented flow analyser (SEAL Analytical Inc. AA500) following the protocol from Aminot and Kérouel (2007). The detection limits were 0.1  $\mu$ M for NO<sub>x</sub>, 0.05  $\mu$ M for DIP and 0.03  $\mu$ M for DSi. Accuracy was checked with certified reference material for nutrients in seawater (KANISO Technos Co.) within 1.4% for NO<sub>x</sub> and DIP and 1.7% for DSi.

## 2.6 Computations, statistical analyses and numerical tools

170 In this study, the size structure of primary production and pigments – including the biomass with TChl*a* – was determined from the bulk and size-fractionated measurements (< 3  $\mu$ m and < 20  $\mu$ m). Picophytoplankton (< 3  $\mu$ m) NPP and pigments were obtained directly from the < 3  $\mu$ m fraction. Nanophytoplankton (3–20  $\mu$ m) NPP and pigments were obtained by





subtracting the  $< 20 \mu\text{m}$  fraction from the  $< 3 \mu\text{m}$  fraction. Microphytoplankton ( $> 20 \mu\text{m}$ ) NPP and pigments were obtained by subtracting the total fraction from the  $< 20 \mu\text{m}$  fraction. To best represent the data within the productive layer, biogeochemical parameters in this study were integrated from the surface (0 m) down to the  $Z_{\text{EL}0.01\%}$ , as previous studies have reported significant primary production below the  $Z_{\text{EL}1\%}$  (e.g. Cavagna et al., 2015). The detailed explanation for the choice of the  $Z_{\text{EL}0.01\%}$  is presented in the Supplement (Text S1 and S2; Tables S1 and S2; Fig. S1). Values at 0 m were extrapolated from those at the first sampled depth ( $\sim 10 \text{ m}$ ).

For each size-fractionated parameter (e.g. NPP, TChla, phytoplankton chemotaxonomic group biomass), the relative contributions of each size class averaged across the study area were compared using a one-way ANOVA followed by a post-hoc Tukey test. When normality and homoscedasticity assumptions were not respected, a Kruskal-Wallis test was applied followed by a post-hoc Dunn test. Spearman's rank correlations were performed to assess statistical relationships between biogeochemical parameters based on the volumetric data, as not all volumetric datasets met the normality and homoscedasticity assumptions. Principal component analysis (PCA) was performed on the volumetric dataset ( $n = 72$ ) to investigate the role of environmental parameters (explanatory variables) on the phytoplankton chemotaxonomic groups (supplementary descriptors). Explanatory variables were sea surface temperature (SST), sea surface salinity (SSS),  $\sigma_t$ , dissolved oxygen, PAR, DIC,  $\text{NO}_x$ , DIP, DSi,  $Z_{\text{SML}}$  and  $Z_{\text{EL}0.01\%}$ . Collinearity of explanatory variables was checked using the variance inflation factors (VIFs): explanatory variables with the highest VIFs (SST, SSS, dissolved oxygen, DIP) were removed until all remaining variables had VIF scores  $< 10$ .

All statistical analyses were conducted in the programming environment R 4.4.2 (R Core Team 2024). The package tidyverse (v2.0.0; Wickam et al., 2019) was used for data manipulation; oce (v1.8.3; Kelley & Richards 2024) for trapezoidal integration computations; stats (v4.4.2; R Core Team 2024) and rstatix (v0.7.2; Kassambra 2023) for statistical analyses.

### 3 Results

#### 3.1 Hydrographic and biogeochemical features of the study area

The OISO33-SOCARB transect crossed the three main hydrographic fronts (STF, SAF and PF) which divided the study area into four hydrographic zones (Fig. 1). Located near the PF, stations O10 and E were attributed to the AZ, as the temperature minimum at 200 m reached  $2^\circ\text{C}$  for O10 and was  $< 2^\circ\text{C}$  for E (Belkin and Gordon, 1996). A detailed analysis of the fronts position is presented in the Supplement (Text S3).

The study area can be further subdivided into distinct biogeochemical regions, with contrasting surface TChla and nutrient concentrations in the SML (Table 1). In the STZ, stations O2, O3 and O16 exhibited LNLC conditions, with very low surface TChla; the  $\text{NO}_x/\text{DIP}$  ratios in the SML were notably lower than the Redfield ratio (16/1; Redfield, 1958), indicating a potential N limitation of the phytoplankton activity. Station O11 in the AZ featured HNLC conditions, with low surface TChla despite high macronutrient concentrations; the  $\text{NO}_x/\text{DIP}$  and  $\text{DSi}/\text{NO}_x$  ratios in the SML were close to their optimal values ( $\text{Si}/\text{N}$  for diatoms =  $1.12 \pm 0.33$ , Brzezinski 1985), suggesting a potential micronutrients limitation. Stations O6, O7, O9 and



O10 shared similar features with O11 but exhibited lower surface DSi concentrations, leading to suboptimal DSi/NO<sub>x</sub> ratios. These stations exhibited HN-LSi-LC conditions, indicating a potential (co-)limitation by Si. Station O14 stood out from the latter HN-LSi-LC stations, exhibiting lower NO<sub>x</sub>, DIP and DSi concentrations in the SML along with a NO<sub>x</sub>/DIP and DSi/NO<sub>x</sub> ratios below the suboptimal values. Stations O12, E and A3, located in the naturally Fe-fertilized Kerguelen bloom (Blain et al., 2008; Qu  rou   et al., 2015), exhibited the highest surface TChl*a* and suboptimal DSi/NO<sub>x</sub> ratios in the SML. These stations were grouped into a region hereafter referred to as “Kerguelen bloom” (KER), which differed from the offshore stations in the PFZ (O6, O7, O9) and AZ (O11, O10) (Table 1).

**Table 1: Metadata, hydrological and biogeochemical features for the SOCARB stations. Stations were grouped according to their hydrographic zone and biogeochemical region. Region assignment was based on surface TChl*a*, nutrient concentrations and molar ratios (mean ± SD) in surface mixed layer (SML).**

METADATA			HYDROLOGY			SURFACE VALUES			SURFACE MIXED LAYER VALUES (MEAN ± SD)						
St.	Zone	Region	Lat. [°S]	Lon. [°E]	Z <sub>SML</sub> [m]	Z <sub>EL1%</sub> [m]	Z <sub>EL0.01%</sub> [m]	SST [°C]	SSS [psu]	TChl <i>a</i> [mg m <sup>-3</sup> ]	NO <sub>x</sub> [��mol L <sup>-1</sup> ]	DIP [��mol L <sup>-1</sup> ]	DSi [��mol L <sup>-1</sup> ]	NO <sub>x</sub> /DIP [mol/mol]	DSi/NO <sub>x</sub> [mol/mol]
O2	STZ	LNLC	30.00	54.10	24	93	185	25.0	35.71	0.07	0.17	0.04	2.19	3.6	13.6
O3	STZ	LNLC	35.00	53.50	14	118	236	20.4	35.53	0.10	0.33	0.11	2.37	3.1	7.3
O16	STZ	LNLC	35.18	73.37	40	90	181	21.3	35.42	0.07	0.11 ± 0.02	0.18 ± 0.02	1.63 ± 0.02	0.6 ± 0.1	15.3 ± 3.9
O14	SAZ	HN-LSi-LC	42.50	74.75	49	87	174	14.5	34.90	0.21	3.72	0.42	1.25	8.9	0.3
O6	PFZ	HN-LSi-LC	45.00	52.27	27	84	168	9.5	33.68	0.15	21.0	1.40	3.77	15.0	0.2
O7	PFZ	HN-LSi-LC	47.67	58.00	30	82	164	8.6	33.73	0.19	19.9	1.38	2.78	14.5	0.1
O9	PFZ	HN-LSi-LC	48.50	65.00	30	83	166	6.1	33.78	0.20	24.9 ± 0.45	1.63 ± 0.03	6.07	15.3 ± 0.1	0.2
O12	PFZ	KER (PFZ)	47.00	72.02	85	46	93	7.5	33.70	0.71	20.1 ± 1.41	1.42 ± 0.10	1.92 ± 0.57	14.1 ± 0.1	0.1 ± 0.0
E	AZ	KER (AZ)	48.80	72.37	82	63	125	4.4	33.89	0.40	25.5 ± 0.30	1.71 ± 0.05	5.72 ± 0.85	15.0 ± 0.5	0.2 ± 0.0
A3	AZ	KER (AZ)	50.50	71.97	108	48	97	4.3	33.91	0.67	25.4 ± 0.94	1.81 ± 0.05	4.16 ± 0.35	14.0 ± 0.2	0.2 ± 0.0
O10	AZ	HN-LSi-LC	50.67	68.42	84	69	137	4.7	33.83	0.30	26.6 ± 0.54	1.75 ± 0.04	8.56 ± 0.41	15.2 ± 0.1	0.3 ± 0.0
O11	AZ	HNLC	56.50	63.00	90	101	203	1.9	33.85	0.17	29.6 ± 0.23	2.04 ± 0.09	27.7	14.6 ± 0.4	0.9

STZ, Subtropical Zone; SAZ, Subantarctic Zone; PFZ, Polar Frontal Zone; AZ, Antarctic Zone; KER, Kerguelen bloom; SST, Sea Surface Temperature; SSS, Sea Surface Salinity; TChl*a*, total chlorophyll *a*; NO<sub>x</sub> = NO<sub>3</sub><sup>-</sup> + NO<sub>2</sub><sup>-</sup>; DIP, dissolved inorganic phosphorus; DSi, dissolved silicon.

## 3.2 Synoptic view of the distribution of phytoplankton biomass and primary production

### 3.2.1 Vertical distribution of TChl*a* and NPP

The TChl*a* profiles of the total fraction (TChl*a*<sub>TOTAL</sub>) and the size classes (TChl*a*<sub>PICO</sub>, TChl*a*<sub>NANO</sub>, TChl*a*<sub>MICRO</sub>) are presented in Fig. 2a-e at five stations, representative of each biogeochemical region (O2 for STZ, O14 for SAZ, O9 for PFZ, O11 for AZ, O12 for KER), and also displayed in Fig. A1 in Appendix A for all stations. At all stations, the SCM of TChl*a*<sub>TOTAL</sub> occurred between 60 and 100 m and was usually below the Z<sub>SML</sub>, except for O12 where the SCM was located at 45 m and above the Z<sub>SML</sub>. At most stations, the SCM depth was similar for the total fraction and the size classes. However, some stations exhibited notable differences. For instance, at O16 (STZ) and O6 (PFZ), the SCM of TChl*a*<sub>PICO</sub> was deeper than that of



TChla<sub>TOTAL</sub> (Fig. A1). Despite vertical variations in TChla, the TChla size structure – *i.e.* the relative contributions of each size class to TChla<sub>TOTAL</sub> – remained unchanged with depth for all stations, except for O11 with TChla dominated by nano- at the surface and by microphytoplankton at the SCM.

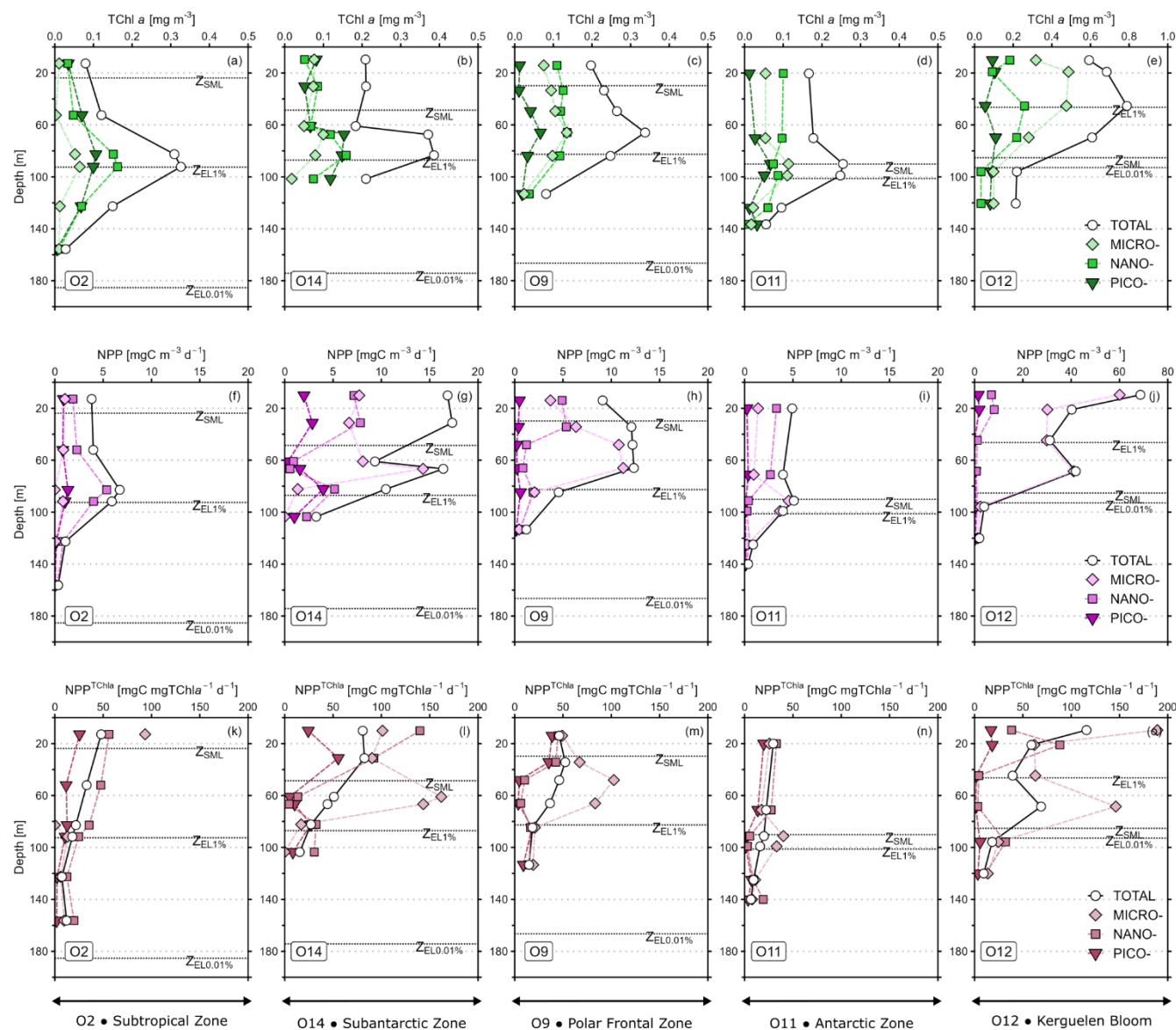


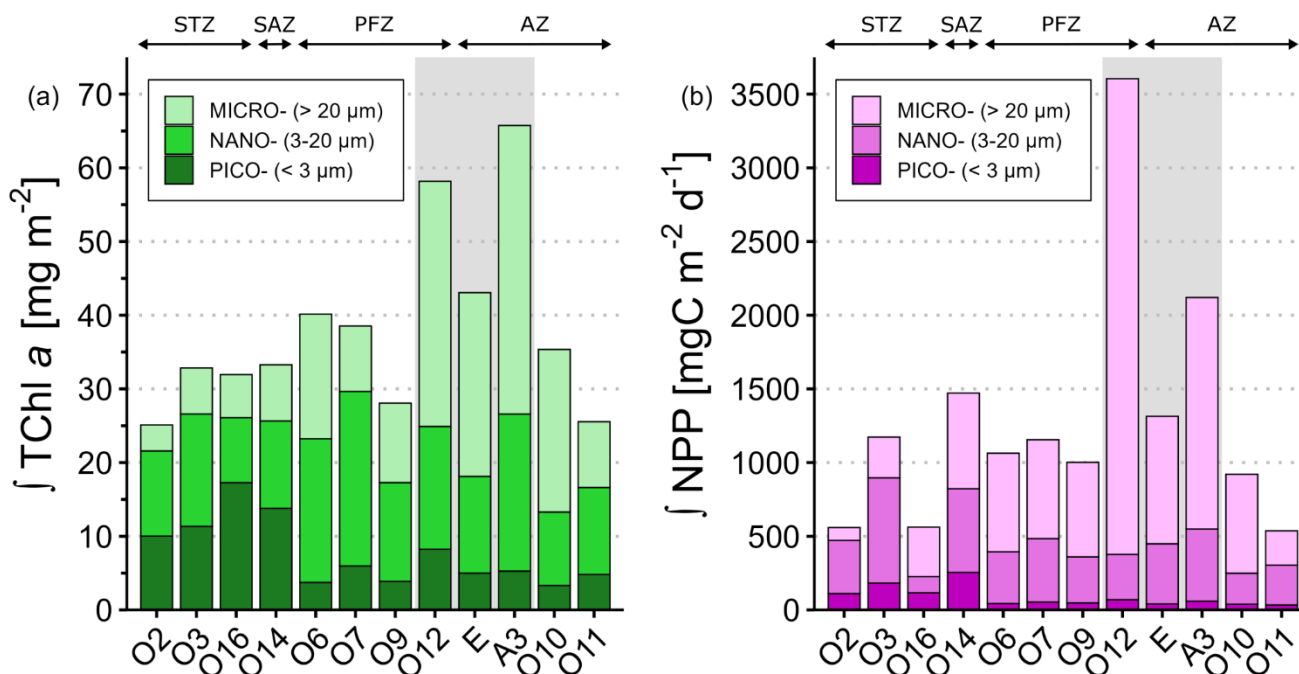
**Figure 2:** Vertical profiles of (a-e) total chlorophyll *a* (TChla), (f-j) net primary production, (k-o) TChla-normalised primary production ( $\text{NPP}^{\text{TChla}}$ ) at five stations located in each hydrographic zone: O2 in the Subtropical zone (a, f, k), O14 in the Subantarctic zone (b, g, l), O9 in the Polar Frontal zone (c, h, m), O11 in the Antarctic zone (d, i, n) and O12 in the Kerguelen bloom (e, j, o). Mind the scale differences at O12 for TChla and NPP. The horizontal dashed lines represent the depth of the surface mixed layer (Z<sub>SML</sub>), the depth of the 1% euphotic layer (Z<sub>EL1%</sub>) and the depth of the 0.01 % euphotic layer (Z<sub>EL0.01%</sub>). All the profiles for every station are presented in Appendix A: Fig. A1 for TChla, Fig. A2 for NPP and Fig. A3 for  $\text{PP}^{\text{TChla}}$ .



As for TChla, the NPP profiles of the total fraction ( $NPP_{TOTAL}$ ) and the size classes ( $NPP_{PICO}$ ,  $NPP_{NANO}$ ,  $NPP_{MICRO}$ ) are presented in Fig. 2f-j at five stations and displayed in Fig. A2 in Appendix A for all stations. Here, the subsurface NPP maximums were not as marked as the SCM. Moreover, the subsurface NPP maximums coincided with SCM at O2 and O3 in the STZ. Contrary to TChla, the NPP size structure – *i.e.* the relative contributions of each size class to  $NPP_{TOTAL}$  – was heterogeneous with depth. In the STZ, surface NPP was evenly distributed in each size class, while subsurface NPP maximum was dominated by one size class. It is noteworthy that subsurface NPP maximums at O2 and O3 were mainly dominated by nanophytoplankton while that of O16 was surprisingly dominated by microphytoplankton. In the SAZ, PFZ and AZ, surface NPP was mainly supported by nano- and microphytoplankton, while subsurface NPP maximum was dominated by microphytoplankton. In the KER region, NPP in the size classes was mainly dominated by microphytoplankton. By normalizing NPP to TChla ( $NPP^{TChla}$ ,  $mgC\ mgTChla^{-1}\ d^{-1}$ ) which can reflect photosynthesis efficiency under given environmental conditions (*e.g.* light/nutrient availability; Cermeño et al., 2005),  $NPP^{TChla}_{TOTAL}$  was maximal in the SML at all stations, except at O3 and O6 where it peaked below the SML, and decreased with depth (Fig. 2k-o; Fig. A3 in Appendix A). Interestingly when considering the size classes,  $NPP^{TChla}_{MICRO}$  often peaked below the SML for several stations in the STZ (O16), the SAZ (O14), the PFZ (O6, O7, O9) and the AZ (O11), while  $NPP^{TChla}_{NANO}$  and  $NPP^{TChla}_{PICO}$  were minimal.

### 3.2.2 Spatial distribution of TChla and NPP

Integrated TChla<sub>TOTAL</sub> over the  $Z_{EL0.01\%}$  ranged from 25.1  $mg\ m^{-2}$  at O2 to 65.7  $mg\ m^{-2}$  at A3 (Fig. 3a). Stations in the KER region displayed the highest TChla<sub>TOTAL</sub> ( $55.7 \pm 11.6\ mg\ m^{-2}$ ), while the remaining stations exhibited lower TChla<sub>TOTAL</sub> ( $32.3 \pm 5.3\ mg\ m^{-2}$ ). Across the study area, nano- and microphytoplankton contributed the most to TChla<sub>TOTAL</sub> and represented respectively 40%  $\pm$  11% and 37%  $\pm$  18% of TChla<sub>TOTAL</sub> (Table S3). It is noteworthy that the picophytoplankton relative contribution to TChla<sub>TOTAL</sub> (23%  $\pm$  16%) was significantly lower than those of nano- and microphytoplankton ( $p < 0.05$ ). In the STZ and SAZ, integrated TChla<sub>TOTAL</sub> was similar and dominated by both pico- and nanophytoplankton, which contributed to 42%  $\pm$  8% and 39%  $\pm$  9% respectively. In the offshore PFZ and AZ, integrated TChla<sub>TOTAL</sub> was similar and dominated by the biomass of nano- (46%  $\pm$  12%) and microphytoplankton (40%  $\pm$  14%). In the KER region, microphytoplankton biomass contributed the most to integrated TChla<sub>TOTAL</sub> (58%  $\pm$  1%). Furthermore, the integrated TChla size structure also varied within specific hydrographic zones. For instance, in the PFZ, integrated TChla at O7 was dominated by nanophytoplankton (61%) while the main contributors at O6 and O9 were nano- (48%) and micro- (40%) (Table S3).



265 **Figure 3: Spatial distribution of the phytoplankton size classes for (a) integrated total chlorophyll  $a$  ( $\int \text{TChl } a$ ) and (b) integrated net primary production ( $\int \text{NPP}$ ) over the  $\text{Z}_{\text{EL}0.01\%}$ . The relative contributions values for  $\int \text{TChl } a$  and  $\int \text{NPP}$  are detailed in Supplement Table S3. Stations were grouped according to their hydrographic zone and biogeochemical region. The grey box covers the stations located in the Kerguelen region. STZ, Subtropical Zone; SAZ, Subantarctic Zone; PFZ, Polar Frontal Zone; AZ, Antarctic Zone.**

The lowest integrated  $\text{NPP}_{\text{TOTAL}}$  over the  $\text{Z}_{\text{EL}0.01\%}$  were observed at O11, O16 and O2 ( $553 \pm 14 \text{ mgC m}^{-2} \text{d}^{-1}$ ), while  
 270 the highest values were recorded at A3 ( $2120 \text{ mgC m}^{-2} \text{d}^{-1}$ ) and O12 ( $3605 \text{ mgC m}^{-2} \text{d}^{-1}$ ) (Fig. 3b). Such differences highlighted the greater variability of  $\text{NPP}_{\text{TOTAL}}$  during SOCARB compared to  $\text{TChl } a_{\text{TOTAL}}$ , with a factor of 6.7 for  $\text{NPP}_{\text{TOTAL}}$  versus 2.7 for  $\text{TChl } a_{\text{TOTAL}}$ . In particular in the STZ, integrated  $\text{NPP}_{\text{TOTAL}}$  at O3 was twice higher than at O2 and O16 (Fig. 3b). Across the study area, microphytoplankton was the main contributor to  $\text{NPP}_{\text{TOTAL}}$  ( $56\% \pm 21\%$ ), followed by nano- ( $35\% \pm 17\%$ ) and picophytoplankton ( $9\% \pm 7\%$ ) (Table S3). The relative contributions of each size class to  $\text{NPP}_{\text{TOTAL}}$  were significantly different  
 275 from each other ( $p < 0.05$ ). The NPP size structure remained homogeneous within the PFZ, AZ and KER region, where microphytoplankton contributed the most to integrated  $\text{NPP}_{\text{TOTAL}}$  ( $66\% \pm 13\%$ ), except at O11 where nano- and microphytoplankton accounted respectively for 50% and 43%. The STZ was the sole zone with notable heterogeneity: while nanophytoplankton dominated at the western stations O2 and O3 (mean contribution of 63%), microphytoplankton was the main contributor to integrated  $\text{NPP}_{\text{TOTAL}}$  at the eastern station O16 (60%).

280 Across the global study area, correlations between the total fraction and each size class were significant for both  $\text{TChl } a$  and NPP (Table 2).  $\text{TChl } a_{\text{TOTAL}}$  exhibited the strongest correlations with  $\text{TChl } a_{\text{MICRO}}$  ( $\rho = 0.87$ ) and  $\text{TChl } a_{\text{NANO}}$  ( $\rho = 0.80$ ), while  $\text{NPP}_{\text{TOTAL}}$  was most strongly correlated with  $\text{NPP}_{\text{MICRO}}$  ( $\rho = 0.86$ ). When comparing the hydrographic zones, both



TChla and NPP correlations revealed a clear spatial variability. In the STZ, the total fraction displayed the highest correlations with pico- and nanophytoplankton, while in the PFZ, AZ and KER region it correlated most strongly with nano- and microphytoplankton. NPP<sub>TOTAL</sub> was significantly correlated with TChla for each size class over the global study area, with the strongest correlations found with TChla<sub>NANO</sub> ( $p = 0.76$ ) and TChla<sub>MICRO</sub> ( $p = 0.70$ ). When comparing the hydrographic zones, TChla<sub>PICO</sub> had a significant impact on NPP<sub>TOTAL</sub> only in the STZ, while TChla<sub>NANO</sub> and TChla<sub>MICRO</sub> had a significant impact on NPP<sub>TOTAL</sub> in each hydrographic zone. The SAZ was the sole exception, as no significative correlations were found between NPP<sub>TOTAL</sub> and TChla in any size class, likely due to the small number of samples.

**Table 2: Spearman's rank correlation coefficients of volumetric TChla and NPP for the different size classes (total, pico-, nano- and micro-) in the global study area and within the different zones. Significant results are presented in bold font.**

Area	Global study area	STZ	SAZ	PFZ	AZ	KER
Stations		O2; O3; O16	O14	O6; O7; O9	O10; O11	O12; A3; E
	n = 72	n = 18	n = 6	n = 18	n = 12	n = 18
TChla <sub>TOTAL</sub> vs. TChla <sub>PICO</sub>	<b>0.49 ***</b>	<b>0.94 ***</b>	0.70	<b>0.76 ***</b>	0.52	0.41
TChla <sub>TOTAL</sub> vs. TChla <sub>NANO</sub>	<b>0.80 ***</b>	<b>0.92 ***</b>	<b>0.93 **</b>	<b>0.82 ***</b>	<b>0.66 *</b>	<b>0.85 ***</b>
TChla <sub>TOTAL</sub> vs. TChla <sub>MICRO</sub>	<b>0.87 ***</b>	<b>0.77 ***</b>	0.61	<b>0.87 ***</b>	<b>0.93 ***</b>	<b>0.95 ***</b>
PP <sub>TOTAL</sub> vs. PP <sub>PICO</sub>	<b>0.32 **</b>	<b>0.56 *</b>	0.60	0.20	0.48	0.35
PP <sub>TOTAL</sub> vs. PP <sub>NANO</sub>	<b>0.58 ***</b>	<b>0.61 **</b>	0.60	0.29	<b>0.68 *</b>	<b>0.50 *</b>
PP <sub>TOTAL</sub> vs. PP <sub>MICRO</sub>	<b>0.86 ***</b>	0.45	0.31	<b>0.89 ***</b>	<b>0.92 ***</b>	<b>0.97 ***</b>
PP <sub>TOTAL</sub> vs. TChla <sub>PICO</sub>	<b>0.30 *</b>	<b>0.57 *</b>	-0.31	0.33	0.31	0.43
PP <sub>TOTAL</sub> vs. TChla <sub>NANO</sub>	<b>0.76 ***</b>	<b>0.82 ***</b>	0.03	<b>0.53 *</b>	<b>0.69 *</b>	<b>0.77 ***</b>
PP <sub>TOTAL</sub> vs. TChla <sub>MICRO</sub>	<b>0.70 ***</b>	<b>0.79 ***</b>	0.49	<b>0.47 *</b>	<b>0.80 **</b>	<b>0.82 ***</b>

**Significance level: \* for  $< 0.05$ ; \*\* for  $< 0.01$ ; \*\*\* for  $< 0.001$ . STZ, Subtropical Zone; SAZ, Subantarctic Zone; PFZ, Polar Frontal Zone; AZ, Antarctic Zone; KER, Kerguelen region.**

### 3.3 In-depth description of the distribution of the phytoplankton community

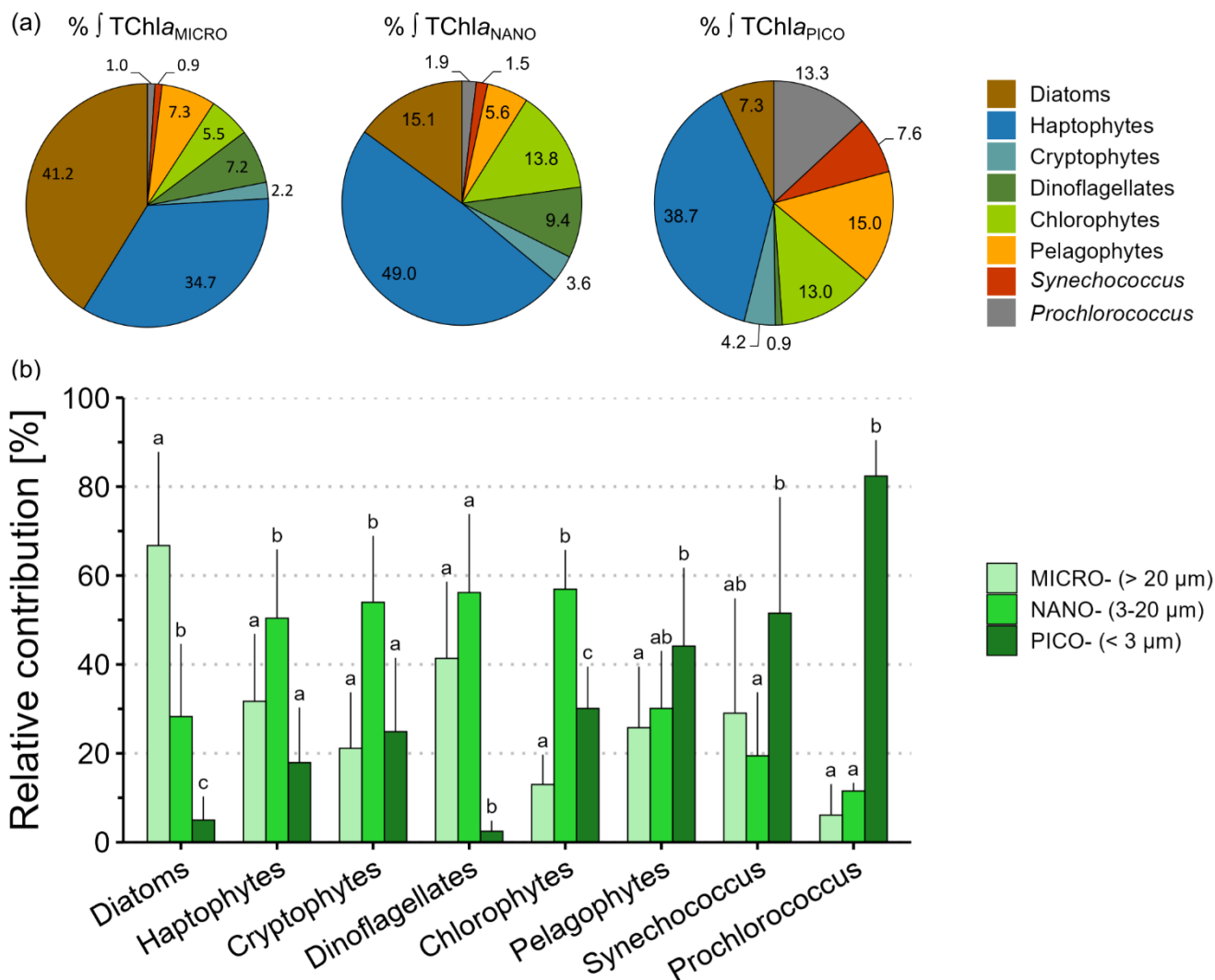
The concentrations and relative contributions of the 8 main accessory pigments (Fuco, Peri, Hex-fuco, But-fuco, Allo, Chlb, Zea and DVChla) integrated over the  $Z_{EL0.01\%}$  for the total fraction and the size classes are presented in the Supplement (Table S4; Fig. S2).

#### 3.3.1 Insights into the biomass and size structure of phytoplankton chemotaxonomic groups across the study area

Over the study area, the main contributors to integrated TChla<sub>TOTAL</sub> were microphytoplankton diatoms ( $20\% \pm 18\%$ ) followed by nanophytoplankton haptophytes ( $19\% \pm 7\%$ ) and microphytoplankton haptophytes ( $14\% \pm 11\%$ ; Table S5). Focusing on the contributions of phytoplankton chemotaxonomic groups biomass to integrated TChla for each size class (Fig. 4a), haptophytes stood out in the three size classes, constituting the dominant and ubiquitous group among all size classes



305 across the study area (Fig. 4a). Focusing on the contributions of each size class to the biomass of the chemotaxonomic groups  
averaged over the study area (Fig. 4b), each chemotaxonomic group was distributed among each size class with contrasting  
relative contributions. Diatoms biomass was mostly associated with the microphytoplankton, accounting for  $67\% \pm 21\%$  of  
total diatoms biomass. Haptophytes, cryptophytes and chlorophytes biomass were mostly found in the nanophytoplankton,  
while dinoflagellates biomass was distributed evenly and almost exclusively in the nano- and microphytoplankton.  
310 Pelagophytes biomass was mainly found in the picophytoplankton, yet nano- and microphytoplankton contributions to total  
pelagophytes biomass remained notable. As expected, cyanobacteria (*Prochlorococcus* and *Synechococcus*) biomass was  
mainly distributed in the picophytoplankton, but also surprisingly detected in the nano- and microphytoplankton.





315 **Figure 4: Insights into the size structure of phytoplankton chemotaxonomic groups using integrated biomass over the  $Z_{EL0.01\%}$  across the global study area ( $n = 12$ ). (a) Circular diagrams of average relative contributions (%) of phytoplankton chemotaxonomic groups to integrated TChl $a$  for the micro-, the nano- and the picophytoplankton size classes. (b) Barplots of average relative contributions (%) of the size classes to the biomass of each phytoplankton chemotaxonomic group. Vertical bars indicate mean relative contribution + SD. Within a given group, mean relative contribution that are not significantly different ( $p \geq 0.05$ ) are labelled with the same letter. Note that *Prochlorococcus* data in the barplots were computed from the STZ and SAZ ( $n = 4$ ), i.e. only where**  
 320 ***Prochlorococcus* biomass was detected.**

### 3.3.2 Spatial distribution of integrated phytoplankton chemotaxonomic groups biomass

In the STZ, where integrated TChl $a_{TOTAL}$  was dominated by pico- ( $43\% \pm 10\%$ ) and nanophytoplankton ( $40\% \pm 11\%$ ), TChl $a_{PICO}$  was dominated by cyanobacteria ( $70\% \pm 13\%$ ) whereas TChl $a_{NANO}$  was mainly sustained by haptophytes ( $43\% \pm 4\%$ ) and chlorophytes ( $20\% \pm 9\%$ ) (Fig. 5e and 5f). In the SAZ, despite similar TChl $a$  size structure compared to STZ,  
 325 TChl $a_{PICO}$  was mainly driven by haptophytes ( $32\%$ ) and pelagophytes ( $30\%$ ) while TChl $a_{NANO}$  was mainly sustained by chlorophytes ( $43\%$ ) and haptophytes ( $30\%$ ). In the offshore PFZ and AZ where integrated TChl $a_{TOTAL}$  was dominated by nano- ( $46\% \pm 12\%$ ) and microphytoplankton ( $40\% \pm 14\%$ ), TChl $a_{NANO}$  was firstly sustained by haptophytes ( $58\% \pm 5\%$ ) followed by diatoms ( $19\% \pm 8\%$ ), whereas TChl $a_{MICRO}$  was firstly driven by diatoms ( $55\% \pm 19\%$ ) followed by haptophytes ( $29\% \pm 10\%$ ) (Fig. 5d-e). In the KER region where TChl $a_{TOTAL}$  was dominated by microphytoplankton ( $58\% \pm 1\%$ ), TChl $a_{MICRO}$  was  
 330 dominated by diatoms and haptophytes whose relative contributions were respectively  $54\% \pm 9\%$  and  $35\% \pm 2\%$  (Fig. 5d).



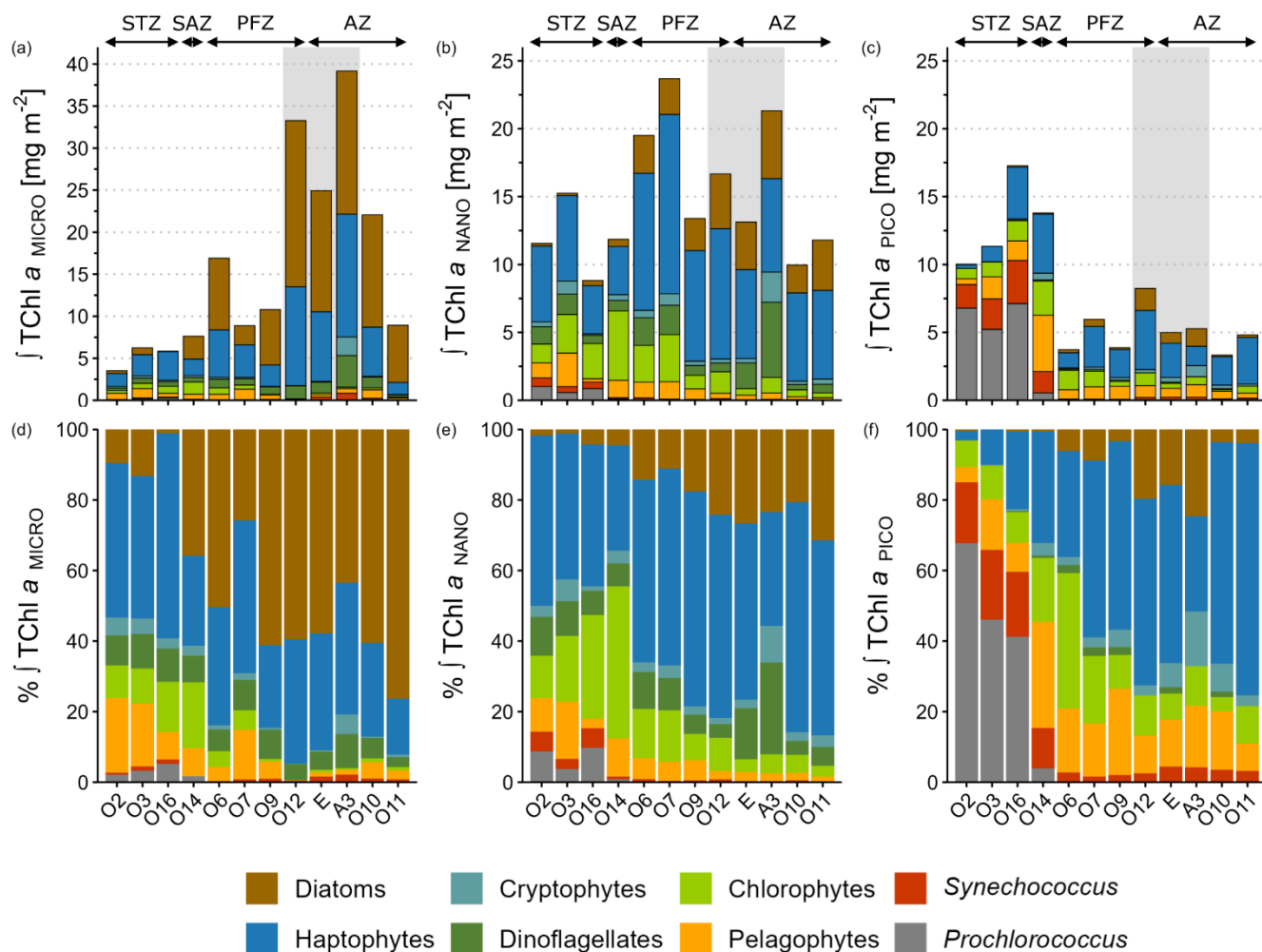


**Figure 5: Spatial distribution of phytoplankton taxonomic groups of (a-c) integrated TChla and (d-f) relative contribution to integrated TChla over the  $Z_{EL0.01\%}$  for the micro- (a, d), the nano- (b, e) and the picophytoplankton (c, f) size classes. Mind the scale differences of TChla for the microphytoplankton compared to nano- and pico-. Stations were grouped according to their hydrographic zone and biogeochemical region. The grey box covers the stations located in the Kerguelen region. STZ, Subtropical Zone; SAZ, Subantarctic Zone; PFZ, Polar Frontal Zone; AZ, Antarctic Zone.**

The size structure of phytoplankton chemotaxonomic groups biomass shifted within each size class across the study area. The microphytoplankton community shifted from haptophyte dominance in the STZ ( $48 \pm 9\%$  of  $TChla_{MICRO}$ ) towards diatom dominance in the PFZ, AZ and KER ( $54 \pm 15\%$ ) (Fig. 5d). Within the nanophytoplankton, chlorophytes were the secondary contributors in the STZ ( $20\% \pm 9\%$  of  $TChla_{NANO}$ ), but were replaced by diatoms in the PFZ, AZ and KER region ( $21 \pm 7\%$ ) (Fig. 5e). The picophytoplankton community shifted from cyanobacteria dominance in the STZ ( $70 \pm 13\%$  of  $TChla_{PICO}$ ) to haptophyte dominance in the PFZ and AZ ( $50 \pm 15\%$ ) (Fig. 5f). This shift across the study area was also observed for the total fraction (Fig. S3). Indeed, the SAZ acted as a “boundary zone” within the study area, delineating distinct



community structures. North of the SAZ, the community in the STZ appeared relatively diversified, with four groups (cyanobacteria, haptophytes, chlorophytes and pelagophytes) each contributing more than 10% to  $TChla_{TOTAL}$ . In contrast, south of the SAZ, the community in the PFZ, AZ and KER region appeared relatively less diversified, with only two groups (diatoms and haptophytes) contributing more than 10 % to  $TChla_{TOTAL}$  (Fig. S3b). In the SAZ, the community at O14 was relatively diversified, with four groups (haptophytes, chlorophytes, pelagophytes and diatoms) each contributing more than 10% to  $TChla_{TOTAL}$ , alongside a marked increase in diatom biomass and a concurrent decline in cyanobacteria.

### 3.4 Links between the size structure of phytoplankton chemotaxonomic groups biomass and primary production

Correlation coefficients were computed between volumetric  $NPP_{TOTAL}$  and phytoplankton chemotaxonomic groups biomass for each size class (Table 3). Across the study area,  $NPP_{TOTAL}$  was mainly driven by the biomass of nano- and microphytoplankton (Table 2). For these two size classes,  $NPP_{TOTAL}$  showed the highest correlation coefficients with the biomass of haptophytes, dinoflagellates and diatoms. In the STZ,  $NPP_{TOTAL}$  was significantly correlated with  $TChla$  in all size classes (Table 2), specifically with the  $TChla_{PICO}$  of cyanobacteria (*Prochlorococcus* and *Synechococcus*) and chlorophytes; with the  $TChla_{NANO}$  of haptophytes, dinoflagellates and chlorophytes; and with the  $TChla_{MICRO}$  of dinoflagellates, haptophytes and diatoms (Table 3). No significant correlations were found in the SAZ. In the PFZ,  $NPP_{TOTAL}$  was significantly correlated with  $TChla_{NANO}$  and  $TChla_{MICRO}$  (Table 2), specifically with the  $TChla_{NANO}$  of diatoms, haptophytes and *Synechococcus*, and with the  $TChla_{MICRO}$  of diatoms, and negatively correlated with the  $TChla_{MICRO}$  of *Synechococcus*. In the AZ and KER region, similar correlation patterns were observed:  $NPP_{TOTAL}$  was mainly correlated with the  $TChla_{NANO}$  of haptophytes and by the  $TChla_{MICRO}$  of haptophytes, diatoms and dinoflagellates (Table 3).

**Table 3: Spearman's rank correlation coefficients between volumetric  $NPP_{TOTAL}$  and the phytoplankton chemotaxonomic groups biomass for each size class following the different zones and regions of the study area. Significant results are presented in bold font.**

Area	Global study area	STZ	SAZ	PFZ	AZ	KER
Stations		O2; O3; O16	O14	O6; O7; O9	O10; O11	O12; A3; E
	n = 72	n = 18	n = 6	n = 18	n = 12	n = 18
<b><i>Prochlorococcus</i></b>						
$NPP_{TOTAL}$ vs. <i>Prochlorococcus</i> <sub>PICO</sub>	-0.18	<b>0.54 *</b>	0.14	NA	NA	NA
$NPP_{TOTAL}$ vs. <i>Prochlorococcus</i> <sub>NANO</sub>	-0.05	0.45	0.15	NA	NA	NA
$NPP_{TOTAL}$ vs. <i>Prochlorococcus</i> <sub>MICRO</sub>	-0.05	0.12	-0.03	NA	NA	NA
<b><i>Synechococcus</i></b>						
$NPP_{TOTAL}$ vs. <i>Synechococcus</i> <sub>PICO</sub>	<b>0.30 *</b>	<b>0.76 ***</b>	0.49	<b>0.88 ***</b>	<b>0.65 *</b>	<b>0.65 **</b>
$NPP_{TOTAL}$ vs. <i>Synechococcus</i> <sub>NANO</sub>	<b>0.37 **</b>	0.41	0.38	<b>0.48 *</b>	0.22	<b>0.65 **</b>
$NPP_{TOTAL}$ vs. <i>Synechococcus</i> <sub>MICRO</sub>	0.01	0.08	NA	<b>-0.87 ***</b>	0.15	0.17
<b>Pelagophytes</b>						
$NPP_{TOTAL}$ vs. Pelagophytes <sub>PICO</sub>	<b>0.42 ***</b>	0.45	-0.71	0.15	<b>0.67 *</b>	0.34
$NPP_{TOTAL}$ vs. Pelagophytes <sub>NANO</sub>	0.14	0.13	-0.46	-0.05	0.02	0.36
$NPP_{TOTAL}$ vs. Pelagophytes <sub>MICRO</sub>	-0.01	0.37	-0.14	-0.30	0.35	-0.30
<b>Chlorophytes</b>						



NPP <sub>TOTAL</sub> vs. Chlorophytes <sub>PICO</sub>	<b>0.33 **</b>	<b>0.56 *</b>	-0.83	0.22	-0.41	<b>0.78 ***</b>
NPP <sub>TOTAL</sub> vs. Chlorophytes <sub>NANO</sub>	<b>0.44 ***</b>	<b>0.61 **</b>	-0.09	0.17	0.28	<b>0.87 ***</b>
NPP <sub>TOTAL</sub> vs. Chlorophytes <sub>MICRO</sub>	0.18	<b>0.56 *</b>	0.54	0.05	<b>0.74 **</b>	-0.39
<b>Dinoflagellates</b>						
NPP <sub>TOTAL</sub> vs. Dinoflagellates <sub>PICO</sub>	0.18	0.00	0.26	-0.28	0.45	-0.48
NPP <sub>TOTAL</sub> vs. Dinoflagellates <sub>NANO</sub>	<b>0.62 ***</b>	<b>0.71 **</b>	0.54	0.38	<b>0.67 *</b>	0.40
NPP <sub>TOTAL</sub> vs. Dinoflagellates <sub>MICRO</sub>	<b>0.74 ***</b>	<b>0.86 ***</b>	0.31	0.37	<b>0.83 ***</b>	<b>0.70 **</b>
<b>Cryptophytes</b>						
NPP <sub>TOTAL</sub> vs. Cryptophytes <sub>PICO</sub>	<b>0.49 ***</b>	-0.31	-0.31	0.20	<b>0.71 **</b>	0.30
NPP <sub>TOTAL</sub> vs. Cryptophytes <sub>NANO</sub>	<b>0.49 ***</b>	0.39	0.06	0.24	0.22	<b>0.57 *</b>
NPP <sub>TOTAL</sub> vs. Cryptophytes <sub>MICRO</sub>	0.07	0.29	-0.03	-0.26	-0.23	-0.11
<b>Haptophytes</b>						
NPP <sub>TOTAL</sub> vs. Haptophytes <sub>PICO</sub>	<b>0.33 **</b>	0.24	0.20	0.29	0.27	0.11
NPP <sub>TOTAL</sub> vs. Haptophytes <sub>NANO</sub>	<b>0.66 ***</b>	<b>0.82 ***</b>	0.37	<b>0.50 *</b>	<b>0.78 **</b>	<b>0.74 ***</b>
NPP <sub>TOTAL</sub> vs. Haptophytes <sub>MICRO</sub>	<b>0.76 ***</b>	<b>0.82 ***</b>	0.49	0.40	<b>0.88 ***</b>	<b>0.80 ***</b>
<b>Diatoms</b>						
NPP <sub>TOTAL</sub> vs. Diatoms <sub>PICO</sub>	<b>0.48 ***</b>	0.00	0.07	0.33	0.15	<b>0.78 ***</b>
NPP <sub>TOTAL</sub> vs. Diatoms <sub>NANO</sub>	<b>0.53 ***</b>	0.17	-0.14	<b>0.67 **</b>	0.42	<b>0.68 **</b>
NPP <sub>TOTAL</sub> vs. Diatoms <sub>MICRO</sub>	<b>0.57 ***</b>	<b>0.68 **</b>	0.83	<b>0.49 *</b>	<b>0.79 **</b>	<b>0.77 ***</b>

Significance level: \* for < 0.05; \*\* for < 0.01; \*\*\* for < 0.001. STZ, Subtropical Zone; SAZ, Subantarctic Zone; PFZ, Polar Frontal Zone; AZ, Antarctic Zone; KER, Kerguelen region.

## 4 Discussion

### 4.1 Understanding the key aspects of phytoplankton biomass and productivity in association with size structure

#### 4.1.1 Vertical size classes decoupling of NPP<sup>TChla</sup>

At several offshore stations in the STZ (O16), SAZ (O14), PFZ (O6, O7, O9) and AZ (O11), NPP<sup>TChla</sup><sub>MICRO</sub> peaked below the SML while NPP<sup>TChla</sup><sub>NANO</sub> and NPP<sup>TChla</sup><sub>PICO</sub> were minimal (Fig. 2k-o; Fig. A3). These maximums could reflect the adaptability of microphytoplankton in low-light environments to take advantage from the nutrients diapycnal diffusion (Tagliabue et al., 2014). At O6, O9 and O11, diatoms were the main contributor to TChla<sub>MICRO</sub> at these NPP<sup>TChla</sup> maximums. Large diatoms are known to thrive in such environmental niches thanks to their high growth efficiency under low-light conditions (Fisher and Halsey, 2016), their ability to regulate buoyancy (Villareal et al., 1996) and to exploit nutrient pulses through enhanced uptake and storage (Kemp and Villareal, 2013). However, haptophytes were the main contributor to TChla<sub>MICRO</sub> at O16, O14 and O7, where NPP<sup>TChla</sup><sub>MICRO</sub> peaked. For these stations, several hypotheses could explain our results. First, haptophytes have been shown to produce transparent exopolymer particles and form microphytoplankton size aggregates (Riebesell et al., 1995; Leblanc et al., 2009). Second, some *Phaeocystis* species such as *P. globosa* or *P. antarctica* are haptophytes known to form microphytoplankton size colonies from nano- and picophytoplankton size single cells, in response to environmental factors such as high irradiance and iron repletion (Feng et al., 2010; Bender et al., 2018), grazing (Long et al., 2007) or NO<sub>x</sub> limitation (Riegman et al., 1992). We rule out the latter hypothesis for explaining colonies formation at O14



and O7, as they featured HN-LSi-LC conditions. Also, Schlüter et al. (2011) reported during late austral spring that one station (~ 37.5°S, ~ 72.5°E), relatively close to O16 (35.18°S, 73.37°E), was influenced by Southern Ocean waters and mainly sustained by haptophytes biomass. Although O16 exhibited distinct LNLC conditions, we cannot rule out the possibility of a potential Southern Ocean water mass in spring, favouring the formation of *Phaeocystis* colonies and shaping upstream the size structure. Further studies are needed to evaluate the recurrent or exceptional aspect of this outstanding feature and the preceding hypotheses.

#### 4.1.2 Global features of phytoplankton biomass and productivity size structures across the study area

Across the study area, microphytoplankton was the main contributor of  $NPP_{TOTAL}$  ( $56 \pm 12\%$ ) while the main contributors to  $TChla_{TOTAL}$  were nano- ( $40 \pm 11\%$ ) and micro- ( $37 \pm 18\%$ ). Our results in  $TChla$  size structure are in agreement with previous studies conducted during austral summer in the South Atlantic and Atlantic sector of the Southern Ocean (Froneman et al., 2001). However, the  $NPP$  size structure in our study differed from that of  $TChla$ , while Froneman et al. (2001) reported that  $NPP$  displayed similar size structure with  $TChla$ . This concerns especially the microphytoplankton, as its contribution to  $NPP_{TOTAL}$  was superior than of  $TChla_{TOTAL}$ . This result suggest that microphytoplankton could be more efficient in  $CO_2$  fixation than the other size classes, which corroborate with previous studies from *in situ* experiments (Cermeno et al., 2005) and photophysiological models (Uitz et al., 2010). More specifically, the higher microphytoplankton photosynthetic efficiencies might be associated with a higher photochemical efficiency characteristic of certain taxonomic groups such as diatoms (Cermeno et al., 2005). We support this hypothesis as microphytoplankton diatoms formed the main contributor of phytoplankton bulk biomass in our study, by representing 20% of  $TChla_{TOTAL}$  (Table S5).

Pigment chemotaxonomy has constituted a valuable tool for estimating the contribution of phytoplankton groups to  $TChla_{TOTAL}$  and analysing phytoplankton communities (Higgins et al., 2011; Kramer et al., 2024). Yet its application remained limited to the bulk fraction. Our study coupling pigment chemotaxonomy with size fractionation brings novel insights to dive deeper into the size structures of the phytoplankton community and of the phytoplankton chemotaxonomic groups. To our knowledge, Nunes et al. (2019) is the only study using these approaches – with CHEMTAX algorithm and two size classes ( $< 3 \mu m$  and  $> 3 \mu m$ ) – to investigate phytoplankton communities in the surface Atlantic Ocean. Along with the latter study, we raise the importance that each phytoplankton chemotaxonomic group was not strictly associated to one specific size class (Fig. 4). These results underline the limits of phytoplankton functional type approaches used to estimate phytoplankton size structure from bulk measurements (*e.g.* Uitz et al., 2006; Hirata et al., 2011). For instance, diatoms and dinoflagellates, which are commonly associated with the microphytoplankton in these approaches, were also distributed in the pico- and nanophytoplankton (Fig. 4). Indeed, Nunes et al. (2019) demonstrated that phytoplankton functional types approaches using bulk measurements predicted a high proportion of nano- and microphytoplankton in the Atlantic sector of the Southern Ocean, while the size fractionation approach indicated the dominance of picophytoplankton. Furthermore, *Prochlorococcus* and *Synechococcus* were mainly distributed in the picophytoplankton, but were also detected in the nano- and microphytoplankton (Fig. 4). This result, also reported by Nunes et al. (2019), can be explained by the size fractionation methodology, as the  $3 \mu m$



and 20  $\mu\text{m}$  pore sizes may retain a part of these organisms. In addition, zeaxanthin, the pigment attributed to *Synechococcus* in the phytoclass algorithm, is also present in microphytoplankton cyanobacteria such as *Trichodesmium* spp. (Jeffrey et al. 2011) and in low concentrations in some Diatoms under high irradiance (Lohr and Wilhelm, 1999), which could explain the attribution of *Synechococcus* in microphytoplankton.

#### 4.1.3 Inter-zonal spatial variability of phytoplankton biomass and productivity size structures in relation with environmental factors

As expected, the size structures of the integrated biomass and primary production shifted clearly between the oligotrophic subtropical waters and the Southern Ocean waters. Result from multivariate analyses showed that  $\sigma$ , DIC and  $\text{NO}_x$  were the major factors in describing this spatial variability between the different zones (Fig. 6). Indeed, temperature, salinity and macronutrients are known factors to shape phytoplankton biomass and productivity size structure, notably with picophytoplankton usually found in warm and oligotrophic waters (Marañón, 2009). The spatial variability in the size structures of TChla and NPP was also observed in the Atlantic basin (Froneman et al., 2001; Nunes et al., 2019). In our study, the TChla and NPP size structures in the PFZ, AZ and KER were mainly sustained by nano- (TChla:  $40 \pm 12\%$ ; NPP:  $30 \pm 12\%$ ) and microphytoplankton (TChla:  $47 \pm 14\%$ ; NPP:  $66 \pm 13\%$ ), which were consistent with previous studies in the Atlantic and Indian sectors of the Southern Ocean (Froneman et al., 2001, 2004; Seeyave et al., 2007; Uitz et al., 2009). By contrast, the TChla size structure in the STZ was mainly driven by the pico- ( $43 \pm 10\%$ ) and nanophytoplankton ( $40 \pm 10\%$ ). To our knowledge, there is no size-fractionated data for biomass and NPP in the literature in the STZ of the SIO. Nevertheless, our results differed from previous studies in the subtropical Atlantic, where picophytoplankton accounted for 55–75% of TChla<sub>TOTAL</sub> (Froneman et al., 2001; Marañón et al., 2001; Morán et al., 2004). Several hypotheses could explain the discrepancies in TChla size structure, such as regional-scale hydrodynamics, nutrient concentrations or atmospheric inputs (Marañón, 2009). Nevertheless, Zhang et al. (2012) reported a latitudinal variability of TChla size structure in the western Pacific, with picophytoplankton being less dominant in subtropical than in tropical regions. For all that, extensive researches are needed in the SIO to better understand the potential factors in shaping the size structures of phytoplankton biomass and productivity, especially in the STZ.

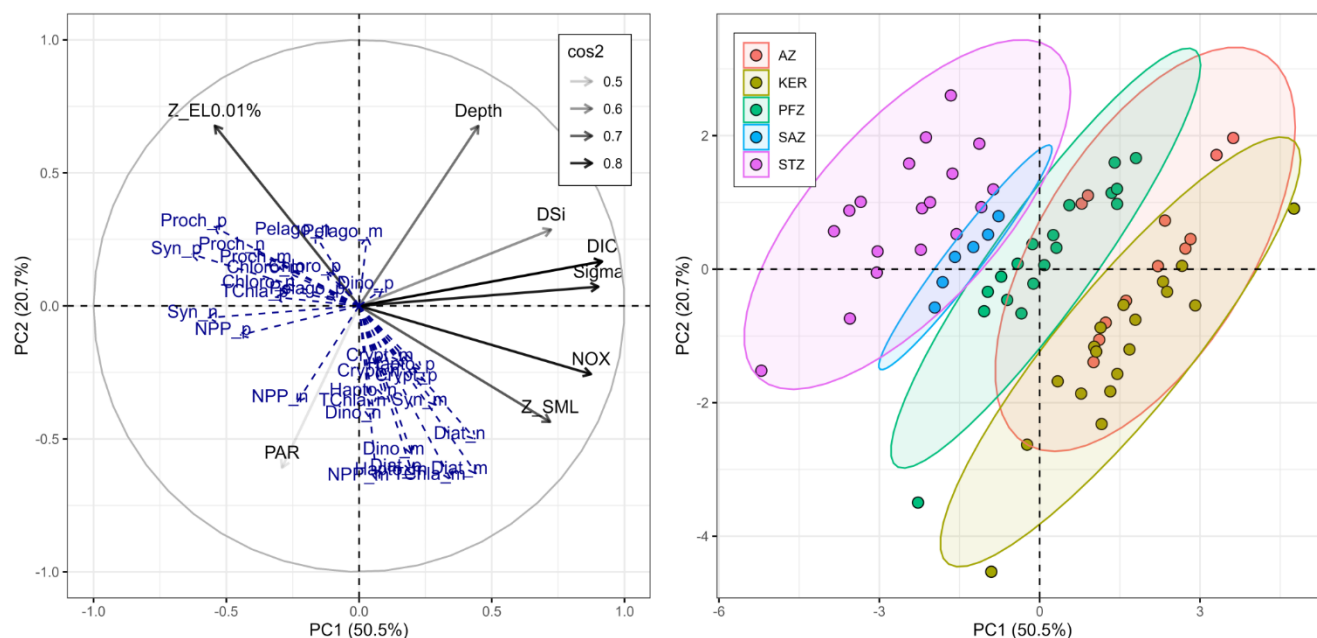


**Figure 6: Principal Component Analysis illustrating the relationships between explanatory variables and supplementary descriptors across the global study area. The first principal component (PC1) axis explains 50.5% of the variance and the second principal component (PC2) axis explains 20.7% of the variance. On the left panel, the black arrows indicate the explanatory variables (environmental factors) with their transparency defined by their  $\cos^2$ : the better the variables are well represented by the principal components, the higher the  $\cos^2$ . The blue arrows show the supplementary descriptors: NPP, TChla and phytoplankton chemotaxonomic groups biomass in each size class. On the right panel, the colour of each point represents the zone of each sample ( $n = 72$ ).**

Phytoplankton chemotaxonomic groups biomass also varied in association with changes in TChla size structure. Cyanobacteria, pelagophytes and chlorophytes mainly sustained picophytoplankton in the STZ – typical for oligotrophic areas with low mixing – while diatoms, haptophytes and dinoflagellates mostly sustained nano- and microphytoplankton in the PFZ, AZ and KER region – typical in areas where these opportunistic taxa are particularly well suited to take advantage of excess nutrient (Fig. 5 and 6) (Schlüter et al., 2011). Also, when focusing on the size structure of phytoplankton chemotaxonomic groups biomass, several common features were observed between Nunes et al. (2019) in the South Atlantic Ocean and our study in the SIO, for similar latitudes. First, we observed that Haptophytes was the main and ubiquitous group within each size class across the SIO; a feature also observed by Nunes et al. (2019) across the Atlantic Ocean. Second, Nunes et al. (2019) reported in the subtropical and tropical Atlantic Ocean the dominance of cyanobacteria in the picophytoplankton (70 % of TChla<sub>PICO</sub>), and the dominance of haptophytes and dinoflagellates in the  $> 3 \mu\text{m}$  fraction (63% of TChla<sub>NANO + MICRO</sub>). These results are in good agreement with ours in the STZ as cyanobacteria represented  $70\% \pm 13\%$  of TChla<sub>PICO</sub> (Fig. 5f) and the sum of haptophytes and dinoflagellates represented  $53 \pm 6\%$  of TChla<sub>NANO</sub> and  $57 \pm 10\%$  of TChla<sub>MICRO</sub> (Fig. 5d and 5e). Third, we observed noteworthy contributions of diatoms to TChla<sub>PICO</sub> in KER ( $20 \pm 4\%$ ; Fig. 5f). Nunes et al. (2019) reported similar





findings in the Atlantic sector of the Southern Ocean in Patagonian waters ( $\sim 40\%$  of  $\text{TChl}_{\text{aPICO}}$ ) and explained this result by the presence of picophytoplankton diatoms and Parmales, a picophytoplankton group genetically very close to diatoms and sharing similar pigments composition (Guillou et al., 1999). This explanation is supported by Deteix et al. (2024) who found that  $< 5 \mu\text{m}$  particles accounted for  $47 \pm 23\%$  of total biogenic silica within the 0–200 m layer in the Indian sector of the Southern Ocean, corroborated by SEM-based identification of picophytoplankton diatoms. Together, these findings across two ocean basins highlight the utility of combining pigment chemotaxonomy with size fractionation to reveal size-specific shifts in phytoplankton communities from subtropical to polar regions. The methodological consistency and alignment of results between these two studies offers promising avenues to refine global assessments of phytoplankton size structure and composition.

## 4.2 Intra-zonal variability of phytoplankton biomass and productivity

### 4.2.1 The Subtropical Zone

Stations O2 and O3, located in the western STZ at similar longitudes, exhibited strong differences in  $\text{TChl}_{\text{a}}$  stocks and NPP fluxes, despite comparable size structures of  $\text{TChl}_{\text{a}}$  and NPP. The integrated  $\text{TChl}_{\text{aTOTAL}}$  and  $\text{NPP}_{\text{TOTAL}}$  at O3 were respectively 31% and 110% higher than at O2, primarily due to increases in the nano- ( $\text{TChl}_{\text{a}}$ : +32%; NPP: + 98%) and microphytoplankton ( $\text{TChl}_{\text{a}}$ : +77%; NPP: +217%) (Fig. 3). However, results from phytoplankton chemotaxonomic groups biomass did not display any noticeable shifts between O2 and O3 (Fig. 5). These differences were likely driven by higher nutrient contents at O3 ( $\text{NO}_x$ : +115%; DIP: +67%;  $\text{DSi}$ : +49%; Table S6). Satellite-derived sea surface height data (GLORYS product) indicated the presence of a cyclonic eddy at O3 characterized by a shallower  $Z_{\text{SML}}$  (Table 1) and nitracline depth than at O2 (data not shown), leading to nutrient upwelling and enhanced productivity and biomass. These hydrographic and biogeochemical features are consistent with previous observations of cyclonic eddies in the Mozambique Channel and Basin (Lamont and Barlow, 2017). Our NPP fluxes are in agreement with previous studies, reporting a 20–100% increase in integrated  $\text{NPP}_{\text{TOTAL}}$  in cyclonic eddies compared to non-eddy areas in the Bay of Bengal (Prasanna Kumar et al., 2007; Sarma et al., 2020) and in the SIO (Dalabehara and Sarma, 2021). Moreover, Sarma et al. (2020) reported no significant differences in the NPP size structure between cyclonic eddy and non-eddy areas, which supports our findings. About  $\text{TChl}_{\text{a}}$ , there is a lack of previous studies focusing on eddies in the Indian Ocean to compare with our dataset. Nevertheless, Vaillancourt et al. (2003) reported a similar 28% increase of integrated  $\text{TChl}_{\text{a}}$  in cyclonic eddy compared to non-eddy areas in the subtropical North Pacific Ocean.

### 4.2.2 The Polar Frontal Zone

Stations O6, O7 and O9 follow a west-east transect, from the Crozet Plateau toward the northwest continental margin of Kerguelen Plateau (Fig. 1). The lower integrated  $\text{TChl}_{\text{aTOTAL}}$  observed at O9 compared to O6 and O7 may be attributed to the island mass effect, where the persistent micronutrients supply downstream of Crozet shape phytoplankton biomass that



decline with distance, as micronutrients become depleted in the SML (Graham et al., 2015; Robinson et al., 2016). Notwithstanding, the TChla size structure at O7 differed from O6 and O9, despite similar NPP<sub>TOTAL</sub> and NPP size structure. Indeed, at O7, the microphytoplankton contribution to TChla<sub>TOTAL</sub> was reduced while that of nano- increased (Fig. 3; Table S3). The decrease in the TChla<sub>MICRO</sub> contribution at O7 was due to the decrease of microphytoplankton diatoms biomass by 4.3–6.2 mg m<sup>-2</sup> compared to O6 and O9 (Fig. 5a). Conversely, the TChla<sub>NANO</sub> contribution increase was caused by the increase of nanophytoplankton haptophytes and chlorophytes biomass by 3.9–7.5 mg m<sup>-2</sup> in comparison to O6 and O9 (Fig. 5b). This community shift corroborated with lower integrated DSi content over the Z<sub>EL0.01%</sub> at O7, on average 60% lower than at O6 and O9 (Table S6). This decrease at O7 likely resulted from a low DSi surface water mass intrusion from the SAZ, leading to the growth limitation of microphytoplankton diatoms in favour of a non-silicifying nanophytoplankton community dominated by haptophytes. This transect is known to be influenced by the southern branch of the SAF current (Park et al., 1993), especially around 55–58°E where a signal of higher SST and lower fCO<sub>2</sub> has been previously observed (Poisson et al., 1993; Leseurre et al., 2022). Indeed, underway continuous measurements during SOCARB recorded an SST increase and fCO<sub>2</sub> decrease between Crozet and O7 around 54–56°E (data not shown).

#### 4.2.3 The Kerguelen bloom area

The highest integrated TChla and NPP at A3 and O12 reflected the well-documented natural Fe fertilization. Despite sharing similar TChla and NPP size structures, integrated NPP displayed variability, as integrated NPP<sub>TOTAL</sub> at A3 was 70% lower compared to O12 (Fig. 3). Previous studies raised potential factors in explaining the variability in integrated NPP in iron-fertilized areas, such as Si availability, phytoplankton community shifts or light-mixing regime (*e.g.* Seeyave et al., 2007). First, A3 and O12 exhibited suboptimal DSi/NO<sub>x</sub> ratios in the SML (Table 1), indicating a potential Si limitation and outlying the Si availability hypothesis. Second, phytoplankton chemotaxonomic groups biomass displayed a noticeable shift in the phytoplankton community structure at A3 compared to O12. The relative contributions of dinoflagellates and cryptophytes to integrated bulk biomass increased by 17% – to the detriment of diatoms and haptophytes by 18% – primarily due to increases in the nanophytoplankton (31%) (Fig. 5; Fig. S3). This shift may not be attributed to the phenology, as satellite-derived surface TChla (MODIS product) did not highlight major differences neither in the timing, nor in the magnitude of phytoplankton biomass (Fig. S4). Third, to investigate the light-mixing regime, we computed the ratio of the diadinoxanthin (DD) and diatoxanthin (DT) concentrations to TChla ((DD+DT):TChla) as an indicator of the mixing processes in the water column (Moline, 1998). Briefly, DD and DT have little chemotaxonomic values but occupy a photoprotective function, with concentrations changing rapidly with irradiance (Demers et al., 1991). Given that most phytoplankton contain DD and DT, the (DD+DT):TChla ratio provides additional information on the vertical mixing rates of the water column along with the light regime (Moline, 1998). The (DD+DT):TChla<sub>TOTAL</sub> ratio at A3 was homogeneous within the SML (Fig. 7a), indicating that the vertical mixing rate was – or had recently been – faster than the photoprotective response (Moline, 1998). Our result corroborated with Uitz et al. (2009), which also studied A3 in late austral summer 2005 and underlined the lack of relationship between the bloom occurrence and the light-mixing regime previously described by Park et al. (2008). In contrary, the



(DD+DT):TChla ratio at O12 decreased with depth within the SML (Fig. 7b), implying that the vertical mixing rate was – or had recently been – slower than the photoprotective response (Moline, 1998). Therefore, the variability in integrated  $NPP_{TOTAL}$  between A3 and O12 could result from contrasting phytoplankton communities and/or light-mixing regimes. Our results highlighted the heterogeneous distribution of phytoplankton communities within the nano- and microphytoplankton size classes in similar productive regimes around the Kerguelen Plateau in late austral summer, which was previously raised only during austral spring by Lasbleiz et al. (2014).

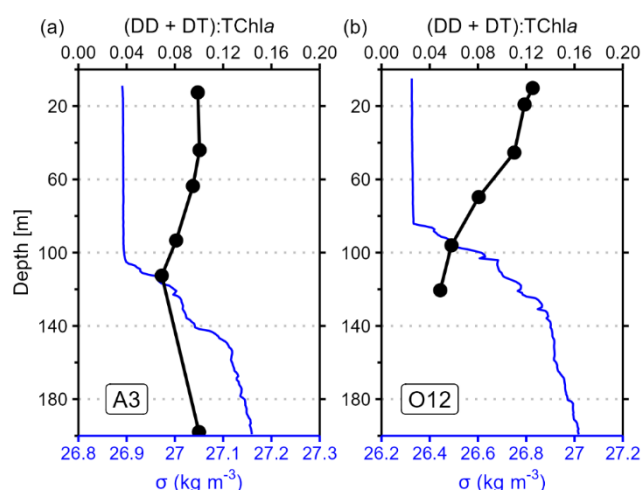


**Figure 7: Vertical profiles of photoacclimation index ((DD + DT):TChla) in black and anomaly density ( $\sigma$ ) in blue for stations A3 (a) and O12 (b).**

### 4.3 Influence of the phytoplankton biomass size structure on NPP

Previously, we demonstrated firstly that  $NPP_{TOTAL}$  was mainly determined by the biomass of nano- and microphytoplankton across the study area, more specifically in the PFZ, AZ and KER region (Table 2), and highlighting their key role in driving  $NPP_{TOTAL}$  in the SIO. Our results are in line with previous studies conducted during austral summer where microphytoplankton biomass drove primary production in iron-fertilised areas, and both nano- and micro- biomass were the drivers of primary production in iron-depleted areas (Froneman et al., 2001, 2004; Korb et al., 2005; Seeyave et al., 2007; Uitz et al., 2009; Shiimoto et al., 2023). However, these studies investigating the relationships between NPP and TChla size structure focused on the Southern Ocean, especially in geographically restricted region (Seeyave et al., 2007; Uitz et al., 2009) or in areas outside the Indian Sector (Froneman et al., 2001, 2004; Korb et al., 2005). While Shiimoto et al. (2023) brings a substantial contribution in the Indian sector of the Southern Ocean south of 60 °S, our study extends these researches northwards of the SIO, up to the SAZ and STZ. Non-significative correlations in the SAZ between  $NPP_{TOTAL}$  and TChla size structure were likely due to the small sample number ( $n = 6$ ), thus limiting any interpretation. Nevertheless, our study showed in the STZ that even though phytoplankton biomass size structure was mainly described by the pico- and nanophytoplankton,



the biomass of each size class would play a significant role in driving  $NPP_{TOTAL}$  (Table 2), including the microphytoplankton despite its small contribution to  $TChla_{TOTAL}$  ( $17 \pm 3\%$ ; Table S3). These results contrast with previous studies in subtropical domains suggesting that  $NPP_{TOTAL}$  was mainly determined by the biomass of pico- and nanophytoplankton (Froneman et al., 2001; Marañón et al., 2001).

Coupling between primary production and phytoplankton community size structure provides an in-depth comprehension of the main phytoplanktonic contributors on the conditioning of NPP. Among the previous studies, Seeyave et al. (2007) and Uitz et al. (2009) investigated the relationships between NPP and phytoplankton community size structure from pigments concentrations. This involves assumptions of the phytoplankton chemotaxonomic affiliation, because certain pigments are major components in many taxa (Higgins et al., 2011). To address this gap, Takao et al. (2012) used satellite data to estimate the spatiotemporal distribution of NPP and four phytoplankton chemotaxonomic groups biomass (*Prochlorococcus*, *Synechococcus*, Haptophytes and Diatoms), from the STZ to the AZ over 1997–2007. Our study fills a gap in this field, as our *in situ* data coupled with the size fractionation approach provide a refined perspective on the phytoplankton community size structure. For instance, among the biomass of nano- and microphytoplankton which drove  $NPP_{TOTAL}$  in the global study area, the biomass of haptophytes, dinoflagellates and diatoms displayed the highest correlations with  $NPP_{TOTAL}$  (Table 3), highlighting the key roles of these chemotaxonomic groups in driving  $NPP_{TOTAL}$  in the SIO. Moreover, the significant correlations of  $NPP_{TOTAL}$  with Diatoms and Haptophytes biomass found in the PFZ, AZ and KER are consistent with the latter studies, but our size fractionation approach underlines the heterogeneity of the relationships in between these zones for each size class (Table 4). Furthermore, while Takao et al. (2012) restricted their study to only four phytoplankton groups biomass due to the limits of the satellite approach, our results showed additional relationships of  $NPP_{TOTAL}$  with the biomass of secondary phytoplankton groups in the AZ and KER such as Chlorophytes, Dinoflagellates and Cryptophytes. Therefore, our findings contribute to a better understanding of the role of phytoplankton community size structure in modulating primary production in the SIO, highlighting that NPP was influenced by the phytoplankton size structure and was not necessarily driven by a single dominant phytoplankton group within a given zone. Additional field studies using the size fractionation approach are needed to complement our current knowledge on the influence of phytoplankton biomass size structure on NPP, especially in the SAZ and STZ where NPP and phytoplankton data remain sparse.

## 5 Conclusion

Using a size fractionation approach, the size structures of phytoplankton algal biomass and primary production were assessed in the SIO during the austral summer 2023, to describe their spatial variability and study the links between primary production and phytoplankton biomass size structure. Across the study area, integrated  $TChla$  size structure was mainly described by the nano- and microphytoplankton size classes, while integrated NPP size structure was dominated by the micro-size class. Furthermore,  $TChla$  size structure exhibited a greater spatial variability compared to NPP size structure. Using the novel pigment chemotaxonomy tool phytoclass (Hayward et al., 2023) coupled with the size fractionation approach, we

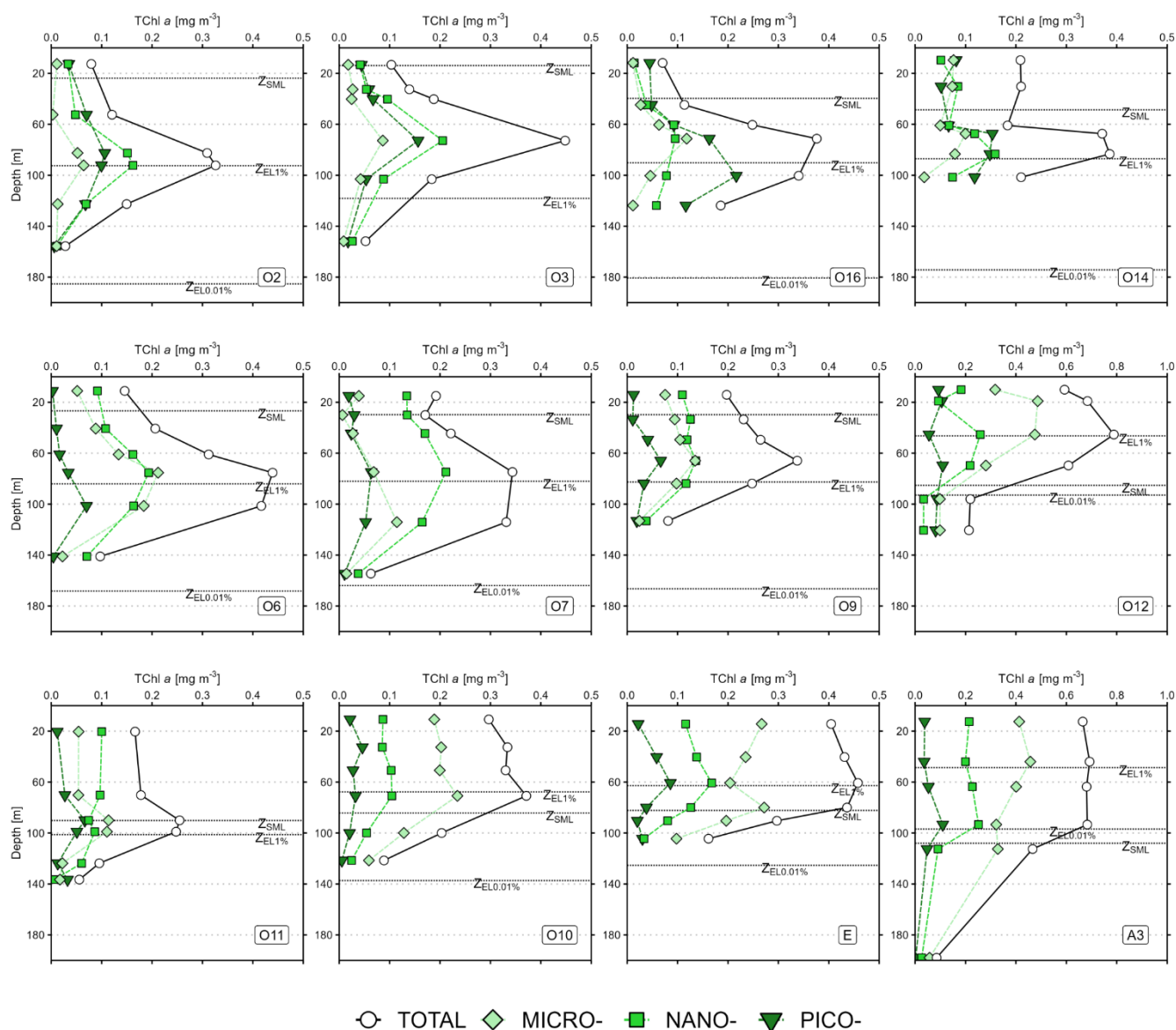


580 determined that haptophytes were the main and ubiquitous group in each size class in the SIO, and that the remaining  
 phytoplankton community shifted within each size class across the SIO. On the one hand, integrated TChla in the STZ was  
 described by pico- and nanophytoplankton, more specifically composed of cyanobacteria (*Prochlorococcus* and  
*Synechococcus*) in the pico- and of haptophytes and chlorophytes in the nanophytoplankton. On the other hand, integrated  
 TChla in the PFZ and AZ was described by nano- and microphytoplankton and featured a community dominated by diatoms  
 585 and haptophytes. Our results also underline the intra-zonal variability of phytoplankton biomass and productivity through  
 bottom-up processes, such as the occurrence of a cyclonic eddy in the STZ or the intrusion of a DSI-depleted water mass in  
 the PFZ. When focusing on the links between NPP and TChla size structure, we demonstrated that  $NPP_{TOTAL}$  was mainly  
 determined by the biomass of nano- and microphytoplankton across the study area, more specifically by the biomass of  
 haptophytes, dinoflagellates and diatoms within these size classes. When deciphering these relationships within each zone, our  
 590 results not only were consistent from previous studies, but also exhibited additional relationships with secondary phytoplankton  
 groups, which could not be identified before due to limitations of previous methodologies.

This study paves the way for a better comprehension of the primary production and phytoplankton community size  
 structure in the SIO, as the size fractionation approach allows to better quantify the impact of the structure and dynamics of  
 the phytoplankton community and their role in the BCP. Furthermore, the concordant results of phytoplankton community size  
 595 structures between Nunes et al. (2019) in the South Atlantic Ocean and this study in the SIO using similar approaches provide  
 promising perspectives in refining the size structure of phytoplankton community at a global scale. In this way, we strongly  
 encourage the marine biogeochemical community, if possible, to use the size fractionation approach to evaluate the  
 phytoplankton community and its associated fluxes. Complementary to SOCARB, these data will be coupled in future works  
 with cytometry and DNA metabarcoding data, to address a more detailed taxonomic description of the phytoplankton  
 600 community, such as evaluating the spatial variability of the community within the haptophytes, which were found in this study  
 to be the main and ubiquitous group in the SIO.

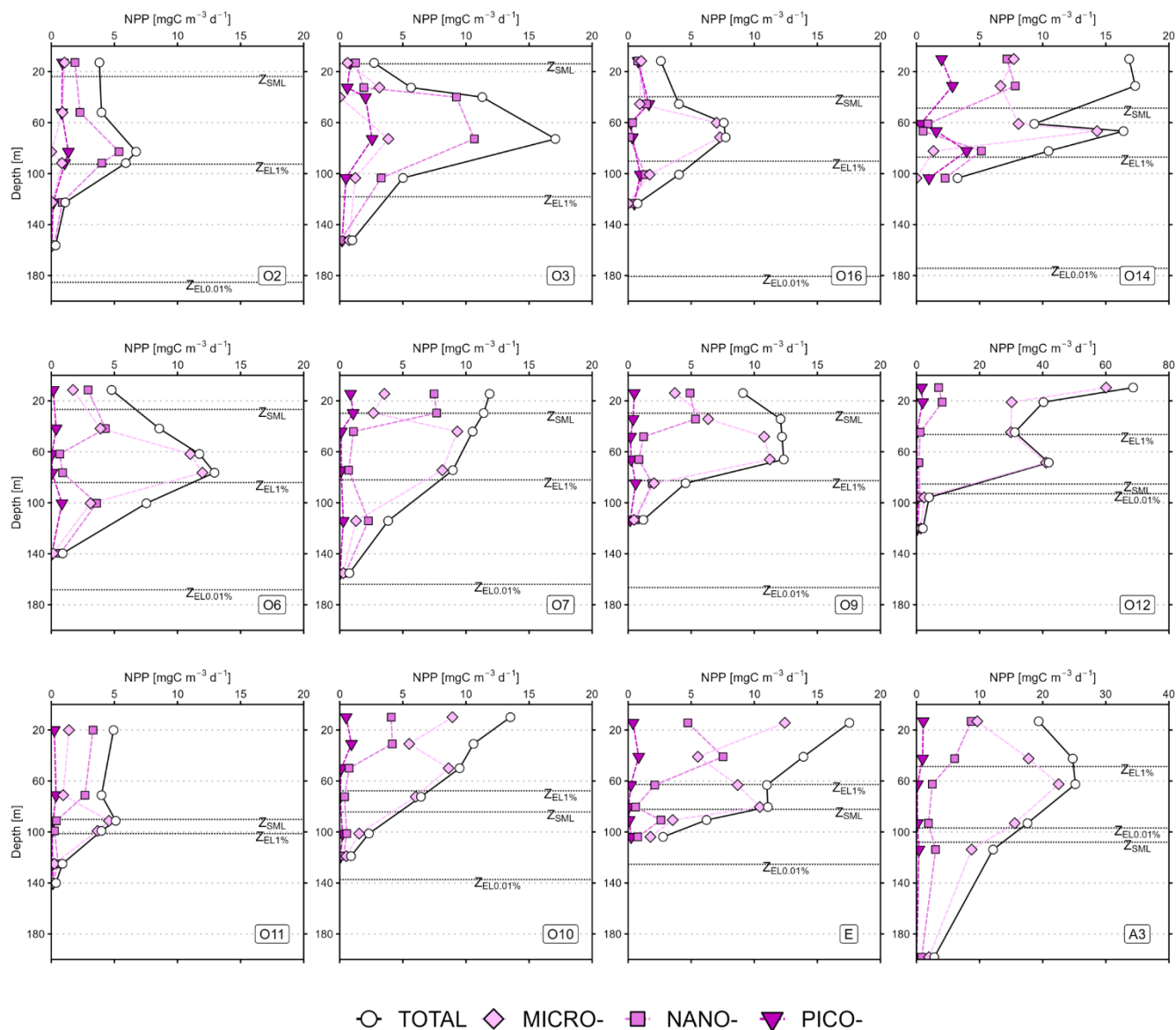


# Appendix A: Vertical profiles of TChl<sub>a</sub>, NPP and TChl<sub>a</sub>-normalized NPP for all SOCARB stations.



605 **Figure A1.** Vertical profiles of total chlorophyll *a* (TChl<sub>a</sub>) at the SOCARB stations. Mind the scale differences at O12 and A3. The dashed lines represent the depth of the mixed layer ( $Z_{SML}$ ), the depth of the 1% euphotic layer ( $Z_{EL1\%}$ ) and the depth of the 0.01 % euphotic layer ( $Z_{EL0.01\%}$ ).





610 **Figure A2. Vertical profiles of net primary production (NPP) for the SOCARB stations. Mind the scale differences at O12 and A3. The dashed lines represent the depth of the mixed layer ( $Z_{SML}$ ), the depth of the 1% euphotic layer ( $Z_{EL1\%}$ ) and the depth of the 0.01 % euphotic layer ( $Z_{EL0.01\%}$ ).**

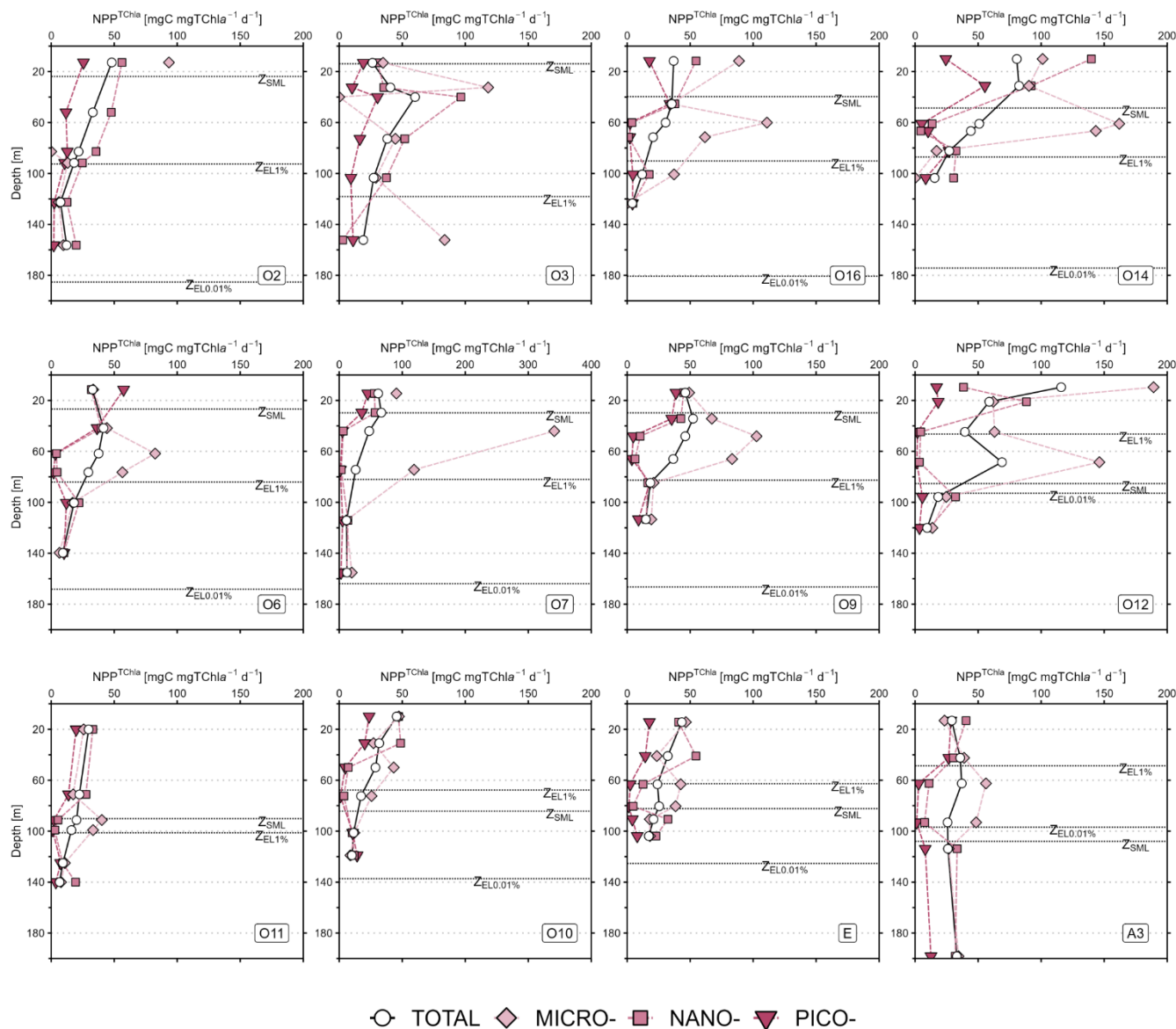


**Figure A3.** Vertical profiles of TChla-normalised net primary production ( $NPP^{TChla}$ ) for the SOCARB stations. Mind the scale differences at O7. The dashed lines represent the depth of the mixed layer ( $Z_{SML}$ ), the depth of the 1% euphotic layer ( $Z_{EL1\%}$ ) and the depth of the 0.01 % euphotic layer ( $Z_{EL0.01\%}$ ).



## Data Availability

Data available in this article will be subsequently submitted to the SEANO database.

## Author contribution

620 **Valentin Deteix:** Formal analysis, investigation, methodology, validation, visualization, writing – original draft. **Céline Ridame:** Conceptualization, formal analysis, funding acquisition, investigation, methodology, supervision, validation, visualization, writing – review and editing. **Celine Dimier:** Investigation, methodology, writing – review and editing. **Claire Lo Monaco:** Funding acquisition, investigation, project administration, writing – review and editing. **Aline Tribollet:** Supervision. **Frédéric Planchon:** Funding acquisition, investigation, project administration, writing – review and editing.

## 625 Competing interests

The authors declare that they have no conflict of interest.

## Acknowledgements

The authors would like to thank the captain C. Souffre and the crew of the R/V *Marion Dufresne II* for their expertise and assistance on board; Fanny Kaczmar for managing clean laboratory and trace metal clean procedures before the cruise; 630 the OISO-33 on board team for nutrients and DIC sampling, and the first DIC analyses on board; Jonathan Fin for DIC analyses at the SNAPO-CO<sub>2</sub> analytical platform (LOCEAN-IPSL); Magloire Mandeng-Yogo and Fethiye Cetin for IR-MS analyses at the Alysés analytical platform (IRD-SU); Eva Delcamp for pigments analyses at the SAPIGH analytical platform (IMEV); the IMAGO analytical platform (IRD) for nutrients analyses. We also thank Nicolas Metzl for his relevant comments on the draft manuscript. This work was part of the PhD's degree research of V. Deteix.

## 635 Financial supports

The SOCARB program was supported by the French Research program of INSU-CNRS LEFE-CYBER (Les Enveloppes Fluides de l'Environnement – Cycles biogéochimiques, environnement et ressources), the ISblue project, Interdisciplinary graduate school for the blue planet (ANR-17-EURE-0015) and co-funded by a grant from the French government under the program "Investissements d'Avenir" embedded in France 2030. The OISO program was supported by 640 the French institutes INSU (Institut National des Sciences de l'Univers), IPEV (Institut Polaire Paul-Émile Victor) and OSU Ecce-Terra (Sorbonne Université), and the French program SOERE/Great-Gases.



## References

- Aminot, A., & K  rouel, R. (Eds.): Dosage automatique des nutriments dans les eaux marines: m  thodes en flux continu. Quae Ifremer, ISBN 978-2-7592-0023-8, 2007.
- 645 Belkin, I. M. and Gordon, A. L.: Southern Ocean fronts from the Greenwich meridian to Tasmania, *Journal of Geophysical Research: Oceans*, 101, 3675–3696, <https://doi.org/10.1029/95JC02750>, 1996.
- Bender, S. J., Moran, D. M., McIlvin, M. R., Zheng, H., McCrow, J. P., Badger, J., DiTullio, G. R., Allen, A. E., and Saito, M. A.: Colony formation in *Phaeocystis antarctica*: connecting molecular mechanisms with iron biogeochemistry, *Biogeosciences*, 15, 4923–4942, <https://doi.org/10.5194/bg-15-4923-2018>, 2018.
- 650 Blain, S., Qu  guiner, B., Armand, L., Belviso, S., Bombled, B., Bopp, L., Bowie, A., Brunet, C., Brussaard, C., Carlotti, F., Christaki, U., Corbi  re, A., Durand, I., Ebersbach, F., Fuda, J.-L., Garcia, N., Gerringa, L., Griffiths, B., Guigue, C., Guillerm, C., Jacquet, S., Jeandel, C., Laan, P., Lef  vre, D., Lo Monaco, C., Malits, A., Mosseri, J., Obernosterer, I., Park, Y.-H., Picheral, M., Pondaven, P., Remenyi, T., Sandroni, V., Sarthou, G., Savoye, N., Scouarnec, L., Souhaut, M., Thuiller, D., Timmermans, K., Trull, T., Uitz, J., van Beek, P., Veldhuis, M., Vincent, D., Viollier, E., Vong, L., and Wagener, T.: Effect of natural iron
- 655 fertilization on carbon sequestration in the Southern Ocean, *Nature*, 446, 1070–1074, <https://doi.org/10.1038/nature05700>, 2007.
- Blain, S., Sarthou, G., and Laan, P.: Distribution of dissolved iron during the natural iron-fertilization experiment KEOPS (Kerguelen Plateau, Southern Ocean), *Deep Sea Research Part II: Topical Studies in Oceanography*, 55, 594–605, <https://doi.org/10.1016/j.dsr2.2007.12.028>, 2008.
- 660 de Boyer Mont  gut, C., Madec, G., Fischer, A. S., Lazar, A., and Iudicone, D.: Mixed layer depth over the global ocean: An examination of profile data and a profile-based climatology, *Journal of Geophysical Research: Oceans*, 109, <https://doi.org/10.1029/2004JC002378>, 2004.
- Browning, T. J., Achterberg, E. P., Engel, A., and Mawji, E.: Manganese co-limitation of phytoplankton growth and major nutrient drawdown in the Southern Ocean, *Nat Commun*, 12, 884, <https://doi.org/10.1038/s41467-021-21122-6>, 2021.
- 665 Brzezinski, M. A.: The Si:C:N ratio of marine diatoms: interspecific variability and the effect of some environmental variables, *Journal of Phycology*, 21, 347–357, <https://doi.org/10.1111/j.0022-3646.1985.00347.x>, 1985.
- Cavagna, A. J., Fripiat, F., Elskens, M., Mangion, P., Chirurgien, L., Closset, I., Lasbleiz, M., Florez-Leiva, L., Cardinal, D., Leblanc, K., Fernandez, C., Lef  vre, D., Oriol, L., Blain, S., Qu  guiner, B., and Dehairs, F.: Production regime and associated N cycling in the vicinity of Kerguelen Island, Southern Ocean, *Biogeosciences*, 12, 6515–6528, [https://doi.org/10.5194/bg-](https://doi.org/10.5194/bg-12-6515-2015)
- 670 12-6515-2015, 2015.
- Cerme  o, P., Est  vez-Blanco, P., Mara  n, E., and Fern  ndez, E.: Maximum photosynthetic efficiency of size-fractionated phytoplankton assessed by <sup>14</sup>C uptake and fast repetition rate fluorometry, *Limnology and Oceanography*, 50, 1438–1446, <https://doi.org/10.4319/lo.2005.50.5.1438>, 2005.



- Cutter, G., Casciotti, K., Croot, P., Geibert, W., Heimbürger, L.-E., Lohan, M., Planquette, H., and van de Flierdt, T.: Sampling  
 675 and Sample-handling Protocols for GEOTRACES Cruises. Version 3, August 2017., 2017.
- Dalabehara, H. B. and Sarma, V. V. S. S.: Physical forcing controls spatial variability in primary production in the Indian  
 Ocean, *Deep Sea Research Part II: Topical Studies in Oceanography*, 183, 104906, <https://doi.org/10.1016/j.dsr2.2020.104906>,  
 2021.
- Demers, S., Roy, S., Gagnon, R., and Vignault, C.: Rapid light-induced changes in cell fluorescence and in xanthophyll-cycle  
 680 pigments of *Alexandrium excavatum* (Dinophyceae) and *Thalassiosira pseudonana* (Bacillariophyceae): a photo-protection  
 mechanism, *Marine Ecology Progress Series*, 76, 185–193, 1991.
- Deteix, V., Cotard, E., Caquineau, S., Landing, W. M., Planchon, F., Ryan-Keogh, T., and Cardinal, D.: Biogenic and  
 lithogenic silicon along the GEOTRACES south West Indian Ocean section (SWINGS-GS02) and the islands mass effect on  
 regional Si biogeochemical cycle, *Marine Chemistry*, 263–264, 104412, <https://doi.org/10.1016/j.marchem.2024.104412>,  
 685 2024.
- Feng, Y., Hare, C. E., Rose, J. M., Handy, S. M., DiTullio, G. R., Lee, P. A., Smith, W. O., Peloquin, J., Tozzi, S., Sun, J.,  
 Zhang, Y., Dunbar, R. B., Long, M. C., Sohst, B., Lohan, M., and Hutchins, D. A.: Interactive effects of iron, irradiance and  
 CO<sub>2</sub> on Ross Sea phytoplankton, *Deep Sea Research Part I: Oceanographic Research Papers*, 57, 368–383,  
<https://doi.org/10.1016/j.dsr.2009.10.013>, 2010.
- 690 Fisher, N. L. and Halsey, K. H.: Mechanisms that increase the growth efficiency of diatoms in low light, *Photosynth Res*, 129,  
 183–197, <https://doi.org/10.1007/s11120-016-0282-6>, 2016.
- Froneman, P. W., Laubscher, R. K., and Mcquaid, C. D.: Size-fractionated Primary Production in the South Atlantic and  
 Atlantic Sectors of the Southern Ocean, *Journal of Plankton Research*, 23, 611–622, <https://doi.org/10.1093/plankt/23.6.611>,  
 2001.
- 695 Froneman, P. W., Pakhomov, E. A., and Balarin, M. G.: Size-fractionated phytoplankton biomass, production and biogenic  
 carbon flux in the eastern Atlantic sector of the Southern Ocean in late austral summer 1997–1998, *Deep Sea Research Part  
 II: Topical Studies in Oceanography*, 51, 2715–2729, <https://doi.org/10.1016/j.dsr2.2002.09.001>, 2004.
- Gandhi, N., Ramesh, R., Laskar, A. H., Sheshshayee, M. S., Shetye, S., Anilkumar, N., Patil, S. M., and Mohan, R.: Zonal  
 variability in primary production and nitrogen uptake rates in the southwestern Indian Ocean and the Southern Ocean, *Deep  
 700 Sea Research Part I: Oceanographic Research Papers*, 67, 32–43, <https://doi.org/10.1016/j.dsr.2012.05.003>, 2012.
- Graham, R. M., De Boer, A. M., van Sebille, E., Kohfeld, K. E., and Schlosser, C.: Inferring source regions and supply  
 mechanisms of iron in the Southern Ocean from satellite chlorophyll data, *Deep Sea Research Part I: Oceanographic Research  
 Papers*, 104, 9–25, <https://doi.org/10.1016/j.dsr.2015.05.007>, 2015.
- Guidi, L., Stemmann, L., Jackson, G. A., Ibanez, F., Claustre, H., Legendre, L., Picheral, M., and Gorsky, G.: Effects of  
 705 phytoplankton community on production, size, and export of large aggregates: A world-ocean analysis, *Limnology and  
 Oceanography*, 54, 1951–1963, <https://doi.org/10.4319/lo.2009.54.6.1951>, 2009.



- Guillou, L., Chrétiennot-Dinet, M.-J., Medlin, L. K., Claustre, H., Goër, S. L., and Vaultot, D.: Bolidomonas: A New Genus with Two Species Belonging to a New Algal Class, the Bolidophyceae (heterokonta), *Journal of Phycology*, 35, 368–381, <https://doi.org/10.1046/j.1529-8817.1999.3520368.x>, 1999.
- 710 Hama, T., Miyazaki, T., Ogawa, Y., Iwakuma, T., Takahashi, M., Otsuki, A., and Ichimura, S.: Measurement of photosynthetic production of a marine phytoplankton population using a stable  $^{13}\text{C}$  isotope, *Mar. Biol.*, 73, 31–36, <https://doi.org/10.1007/BF00396282>, 1983.
- Hauck, J., Gregor, L., Nissen, C., Patara, L., Hague, M., Mongwe, P., Bushinsky, S., Doney, S. C., Gruber, N., Le Quéré, C., Manizza, M., Mazloff, M., Monteiro, P. M. S., and Terhaar, J.: The Southern Ocean Carbon Cycle 1985–2018: Mean, Seasonal  
 715 Cycle, Trends, and Storage, *Global Biogeochemical Cycles*, 37, e2023GB007848, <https://doi.org/10.1029/2023GB007848>, 2023.
- Hawco, N. J., Tagliabue, A., and Twining, B. S.: Manganese Limitation of Phytoplankton Physiology and Productivity in the Southern Ocean, *Global Biogeochemical Cycles*, 36, e2022GB007382, <https://doi.org/10.1029/2022GB007382>, 2022.
- Hayward, A., Pinkerton, M. H., and Gutierrez-Rodriguez, A.: phytoclass: A pigment-based chemotaxonomic method to  
 720 determine the biomass of phytoplankton classes, *Limnology and Oceanography: Methods*, 21, 220–241, <https://doi.org/10.1002/lom3.10541>, 2023.
- Hayward, A., Pinkerton, M. H., Wright, S. W., Gutiérrez-Rodriguez, A., and Law, C. S.: Twenty-six years of phytoplankton pigments reveal a circumpolar Class Divide around the Southern Ocean, *Commun Earth Environ*, 5, 1–7, <https://doi.org/10.1038/s43247-024-01261-6>, 2024.
- 725 Higgins, H. W., Wright, S., & Schluter, L.: Quantitative interpretation of chemotaxonomic pigment data. In: *Phytoplankton Pigments: Characterization, Chemo- Taxonomy and Applications in Oceanography*, edited by: Roy, S., Llewellyn, C., Egeland, E. S., and Johnsen, G., Cambridge University Press, 257–313, ISBN 978-1-107-00066-7, 2011.
- Hirata, T., Hardman-Mountford, N. J., Brewin, R. J. W., Aiken, J., Barlow, R., Suzuki, K., Isada, T., Howell, E., Hashioka, T., Noguchi-Aita, M., and Yamanaka, Y.: Synoptic relationships between surface Chlorophyll-a and diagnostic pigments  
 730 specific to phytoplankton functional types, *Biogeosciences*, 8, 311–327, <https://doi.org/10.5194/bg-8-311-2011>, 2011.
- Holmes, T. M., Wuttig, K., Chase, Z., Schallenberg, C., van der Merwe, P., Townsend, A. T., and Bowie, A. R.: Glacial and Hydrothermal Sources of Dissolved Iron (II) in Southern Ocean Waters Surrounding Heard and McDonald Islands, *Journal of Geophysical Research: Oceans*, 125, e2020JC016286, <https://doi.org/10.1029/2020JC016286>, 2020.
- Hörstmann, C., Raes, E. J., Buttigieg, P. L., Lo Monaco, C., John, U., and Waite, A. M.: Hydrographic fronts shape  
 735 productivity, nitrogen fixation, and microbial community composition in the southern Indian Ocean and the Southern Ocean, *Biogeosciences*, 18, 3733–3749, <https://doi.org/10.5194/bg-18-3733-2021>, 2021.
- Jasmine, P., Muraleedharan, K. R., Madhu, N. V., Devi, C. R. A., Alagarsamy, R., Achuthankutty, C. T., Jayan, Z., Sanjeevan, V. N., and Sahayak, S.: Hydrographic and productivity characteristics along 45°E longitude in the southwestern Indian Ocean and Southern Ocean during austral summer 2004, *Marine Ecology Progress Series*, 389, 97–116,  
 740 <https://doi.org/10.3354/meps08126>, 2009.





- Jeffrey, S. W., Wright, S. W. & Zapata, M.: Microalgal classes and their signature pigments. In: *Phytoplankton Pigments: Characterization, Chemo- Taxonomy and Applications in Oceanography*, edited by: Roy, S., Llewellyn, C., Egeland, E. S., and Johnsen, G., Cambridge University Press, 3-77, ISBN 978-1-107-00066-7, 2011.
- Kassambara A (2023). *\_rstatix: Pipe-Friendly Framework for Basic Statistical Tests\_*. R package version 0.7.2,  
 745 <https://CRAN.R-project.org/package=rstatix>.
- Kelley D, Richards C (2024). *oce: Analysis of Oceanographic Data*. R package version 1.8-3, <https://CRAN.R-project.org/package=oce>
- Kemp, A. E. S. and Villareal, T. A.: High diatom production and export in stratified waters – A potential negative feedback to global warming, *Progress in Oceanography*, 119, 4–23, <https://doi.org/10.1016/j.pocean.2013.06.004>, 2013.
- 750 Korb, R. E., Whitehouse, M. J., Thorpe, S. E., and Gordon, M.: Primary production across the Scotia Sea in relation to the physico-chemical environment, *Journal of Marine Systems*, 57, 231–249, <https://doi.org/10.1016/j.jmarsys.2005.04.009>, 2005.
- Kramer, S. J., Bolaños, L. M., Catlett, D., Chase, A. P., Behrenfeld, M. J., Boss, E. S., Crockford, E. T., Giovannoni, S. J., Graff, J. R., Haëntjens, N., Karp-Boss, L., Peacock, E. E., Roesler, C. S., Sosik, H. M., and Siegel, D. A.: Toward a synthesis of phytoplankton community composition methods for global-scale application, *Limnology and Oceanography: Methods*, 22,  
 755 217–240, <https://doi.org/10.1002/lom3.10602>, 2024.
- Lamont, T., & Barlow, R.: Contrasting hydrography and phytoplankton distribution in the upper layers of cyclonic eddies in the Mozambique Basin and Mozambique Channel, *African Journal of Marine Science*, 39(3), 293–306, <https://doi.org/10.2989/1814232X.2017.1367722>, 2017
- Lasbleiz, M., Leblanc, K., Blain, S., Ras, J., Cornet-Barthaux, V., Hélias Nunige, S., and Quéguiner, B.: Pigments, elemental  
 760 composition (C, N, P, and Si), and stoichiometry of particulate matter in the naturally iron fertilized region of Kerguelen in the Southern Ocean, *Biogeosciences*, 11, 5931–5955, <https://doi.org/10.5194/bg-11-5931-2014>, 2014.
- Latasa, M., Rodríguez, F., Agustí, S., and Estrada, M.: Distribution patterns of phytoplankton groups along isoirradiance layers in oligotrophic tropical and subtropical oceans, *Progress in Oceanography*, 217, 103098, <https://doi.org/10.1016/j.pocean.2023.103098>, 2023.
- 765 Leblanc, K., Quéguiner, B., Fiala, M., Blain, S., Morvan, J., and Corvaisier, R.: Particulate biogenic silica and carbon production rates and particulate matter distribution in the Indian sector of the Subantarctic Ocean, *Deep Sea Research Part II: Topical Studies in Oceanography*, 49, 3189–3206, [https://doi.org/10.1016/S0967-0645\(02\)00078-4](https://doi.org/10.1016/S0967-0645(02)00078-4), 2002.
- Leblanc, K., Hare, C. E., Feng, Y., Berg, G. M., DiTullio, G. R., Neeley, A., Benner, I., Sprengel, C., Beck, A., Sanudo-Wilhelmy, S. A., Passow, U., Klinck, K., Rowe, J. M., Wilhelm, S. W., Brown, C. W., and Hutchins, D. A.: Distribution of  
 770 calcifying and silicifying phytoplankton in relation to environmental and biogeochemical parameters during the late stages of the 2005 North East Atlantic Spring Bloom, *Biogeosciences*, 6, 2155–2179, <https://doi.org/10.5194/bg-6-2155-2009>, 2009.
- Leseurre, C., Lo Monaco, C., Reverdin, G., Metzl, N., Fin, J., Mignon, C., and Benito, L.: Summer trends and drivers of sea surface fCO<sub>2</sub> and pH changes observed in the southern Indian Ocean over the last two decades (1998–2019), *Biogeosciences*, 19, 2599–2625, <https://doi.org/10.5194/bg-19-2599-2022>, 2022.



- 775 Lo Monaco, Metzl, N., and Planchon: OISO-33 cruise, Marion Dufresne R/V, <https://doi.org/10.17600/18002420>, 2023.
- Lohr, M. and Wilhelm, C.: Algae displaying the diadinoxanthin cycle also possess the violaxanthin cycle, *Proceedings of the National Academy of Sciences*, 96, 8784–8789, <https://doi.org/10.1073/pnas.96.15.8784>, 1999.
- Long, J. D., Smalley, G. W., Barsby, T., Anderson, J. T., and Hay, M. E.: Chemical cues induce consumer-specific defenses in a bloom-forming marine phytoplankton, *Proc Natl Acad Sci U S A*, 104, 10512–10517,  
 780 <https://doi.org/10.1073/pnas.0611600104>, 2007.
- Mackey, M., Mackey, D., Higgins, H., and Wright, S.: CHEMTAX - a program for estimating class abundances from chemical markers: application to HPLC measurements of phytoplankton, *Marine Ecology Progress Series*, 144, 265–283, <https://doi.org/10.3354/meps144265>, 1996.
- Maiti, K., Charette, M. A., Buesseler, K. O., and Kahru, M.: An inverse relationship between production and export efficiency  
 785 in the Southern Ocean, *Geophysical Research Letters*, 40, 1557–1561, <https://doi.org/10.1002/grl.50219>, 2013.
- Marañón, E.: Phytoplankton size structure. In: *Encyclopedia of Ocean Sciences*, 2nd Edition, edited by: Steele, J.H., Turekian, K., Thorpe, S.A., Academic Press, Oxford, 2009.
- Marañón, E., Holligan, P. M., Barciela, R., González, N., Mouriño, B., Pazó, M. J., and Varela, M.: Patterns of phytoplankton size structure and productivity in contrasting open-ocean environments, *Marine Ecology Progress Series*, 216, 43–56,  
 790 <https://doi.org/10.3354/meps216043>, 2001.
- Martin, J. H.: Glacial-interglacial CO<sub>2</sub> change: The Iron Hypothesis, *Paleoceanography*, 5, 1–13, <https://doi.org/10.1029/PA005i001p00001>, 1990.
- Martin, J. H., Fitzwater, S. E., and Gordon, R. M.: Iron deficiency limits phytoplankton growth in Antarctic waters, *Global Biogeochemical Cycles*, 4, 5–12, <https://doi.org/10.1029/GB004i001p00005>, 1990.
- 795 McClain, C. R., Signorini, S. R., and Christian, J. R.: Subtropical gyre variability observed by ocean-color satellites, *Deep Sea Research Part II: Topical Studies in Oceanography*, 51, 281–301, <https://doi.org/10.1016/j.dsr2.2003.08.002>, 2004.
- Mendes, C. R. B., Kerr, R., Tavano, V. M., Cavalheiro, F. A., Garcia, C. A. E., Dessai, D. R. G., and Anilkumar, N.: Cross-front phytoplankton pigments and chemotaxonomic groups in the Indian sector of the Southern Ocean, *Deep Sea Research Part II: Topical Studies in Oceanography*, 118, 221–232, <https://doi.org/10.1016/j.dsr2.2015.01.003>, 2015.
- 800 Metzl, N., Poisson, A., Louanchi, F., Brunet, C., Schauer, B., and Bres, B.: Spatio-temporal distributions of air-sea fluxes of CO<sub>2</sub> in the Indian and Antarctic oceans, *Tellus B*, 47, 56–69, <https://doi.org/10.1034/j.1600-0889.47.issue1.7.x>, 1995.
- Metzl, N., Fin, J., Lo Monaco, C., Mignon, C., Alliouane, S., Bombled, B., Boutin, J., Bozec, Y., Comeau, S., Conan, P., Coppola, L., Cuët, P., Ferreira, E., Gattuso, J.-P., Gazeau, F., Goyet, C., Grossteffan, E., Lansard, B., Lefèvre, D., Lefèvre, N., Leseurre, C., Petton, S., Pujo-Pay, M., Rabouille, C., Reverdin, G., Ridame, C., Rimmelín-Maury, P., Ternon, J.-F., Touratier,  
 805 F., Tribollet, A., Wagener, T., and Wimart-Rousseau, C.: An updated synthesis of ocean total alkalinity and dissolved inorganic carbon measurements from 1993 to 2023: the SNAPO-CO<sub>2</sub>-v2 dataset, *Earth System Science Data*, 17, 1075–1100, <https://doi.org/10.5194/essd-17-1075-2025>, 2025.



- Minas, H. and Minas, M.: Net community production in high nutrient-low chlorophyll waters of the tropical and antarctic oceans - grazing vs iron hypothesis, *Oceanologica Acta*, 15, 145–162, 1992.
- 810 Moline, M. A.: Photoadaptive response during the development of a coastal Antarctic diatom bloom and relationship to water column stability, *Limnology and Oceanography*, 43, 146–153, <https://doi.org/10.4319/lo.1998.43.1.0146>, 1998.
- Moore, J. K. and Abbott, M. R.: Phytoplankton chlorophyll distributions and primary production in the Southern Ocean, *Journal of Geophysical Research: Oceans*, 105, 28709–28722, <https://doi.org/10.1029/1999JC000043>, 2000.
- Morán, X. A. G., Fernández, E., and Pérez, V.: Size-fractionated primary production, bacterial production and net community  
 815 production in subtropical and tropical domains of the oligotrophic NE Atlantic in autumn, *Marine Ecology Progress Series*, 274, 17–29, <https://doi.org/10.3354/meps274017>, 2004.
- Morel, A. and Berthon, J.-F.: Surface pigments, algal biomass profiles, and potential production of the euphotic layer: Relationships reinvestigated in view of remote-sensing applications, *Limnology and Oceanography*, 34, 1545–1562, <https://doi.org/10.4319/lo.1989.34.8.1545>, 1989.
- 820 Nelson, D. M., Brzezinski, M. A., Sigmon, D. E., and Franck, V. M.: A seasonal progression of Si limitation in the Pacific sector of the Southern Ocean, *Deep Sea Research Part II: Topical Studies in Oceanography*, 48, 3973–3995, [https://doi.org/10.1016/S0967-0645\(01\)00076-5](https://doi.org/10.1016/S0967-0645(01)00076-5), 2001.
- Nowlin, W. D. and Klinck, J. M.: The physics of the Antarctic Circumpolar Current, *Reviews of Geophysics*, 24, 469–491, <https://doi.org/10.1029/RG024i003p00469>, 1986.
- 825 Nunes, S., Perez, G. L., Latasa, M., Zamanillo, M., Delgado, M., Ortega-Retuerta, E., Marrasé, C., Simó, R., and Estrada, M.: Size fractionation, chemotaxonomic groups and bio-optical properties of phytoplankton along a transect from the Mediterranean Sea to the SW Atlantic Ocean, *Scientia Marina*, 83, 87–109, <https://doi.org/10.3989/scimar.04866.10A>, 2019.
- Park, Y.-H., Gamberoni, L., and Charriaud, E.: Frontal structure, water masses, and circulation in the Crozet Basin, *Journal of Geophysical Research: Oceans*, 98, 12361–12385, <https://doi.org/10.1029/93JC00938>, 1993.
- 830 Park, Y.-H., Fuda, J.-L., Durand, I., and Naveira Garabato, A. C.: Internal tides and vertical mixing over the Kerguelen Plateau, *Deep Sea Research Part II: Topical Studies in Oceanography*, 55, 582–593, <https://doi.org/10.1016/j.dsr2.2007.12.027>, 2008.
- Poisson, A., Metzl, N., Brunet, C., Schauer, B., Bres, B., Ruiz-Pino, D., and Louanchi, F.: Variability of sources and sinks of CO<sub>2</sub> in the western Indian and southern oceans during the year 1991, *Journal of Geophysical Research: Oceans*, 98, 22759–22778, <https://doi.org/10.1029/93JC02501>, 1993.
- 835 Pollard, R. T., Salter, I., Sanders, R. J., Lucas, M. I., Moore, C. M., Mills, R. A., Statham, P. J., Allen, J. T., Baker, A. R., Bakker, D. C. E., Charette, M. A., Fielding, S., Fones, G. R., French, M., Hickman, A. E., Holland, R. J., Hughes, J. A., Jickells, T. D., Lampitt, R. S., Morris, P. J., Nédélec, F. H., Nielsdóttir, M., Planquette, H., Popova, E. E., Poulton, A. J., Read, J. F., Seeyave, S., Smith, T., Stinchcombe, M., Taylor, S., Thomalla, S., Venables, H. J., Williamson, R., and Zubkov, M. V.: Southern Ocean deep-water carbon export enhanced by natural iron fertilization, *Nature*, 457, 577–580,  
 840 <https://doi.org/10.1038/nature07716>, 2009.



- Prasanna Kumar, S., Nuncio, M., Ramaiah, N., Sardesai, S., Narvekar, J., Fernandes, V., and Paul, J. T.: Eddy-mediated biological productivity in the Bay of Bengal during fall and spring intermonsoons, *Deep Sea Research Part I: Oceanographic Research Papers*, 54, 1619–1640, <https://doi.org/10.1016/j.dsr.2007.06.002>, 2007.
- Quéro  , F., Sarthou, G., Planquette, H. F., Bucciarelli, E., Chever, F., van der Merwe, P., Lannuzel, D., Townsend, A. T.,  
 845 Cheize, M., Blain, S., d’Ovidio, F., and Bowie, A. R.: High variability in dissolved iron concentrations in the vicinity of the Kerguelen Islands (Southern Ocean), *Biogeosciences*, 12, 3869–3883, <https://doi.org/10.5194/bg-12-3869-2015>, 2015.
- R Core Team 2024. *\_R: A Language and Environment for Statistical Computing\_*. R Foundation for Statistical Computing, Vienna, Austria, <https://www.R-project.org/>
- Ras, J., Claustre, H., and Uitz, J.: Spatial variability of phytoplankton pigment distributions in the Subtropical South Pacific  
 850 Ocean: comparison between in situ and predicted data, *Biogeosciences*, 5, 353–369, <https://doi.org/10.5194/bg-5-353-2008>, 2008.
- Redfield, A. C.: The Biological Control of Chemical Factors in the Environment, *American Scientist*, 46, 230A–221, 1958.
- Ridame, C., Dinasquet, J., Hallstr  m, S., Bigeard, E., Riemann, L., Van Wambeke, F., Bressac, M., Pulido-Villena, E.,  
 Taillandier, V., Gazeau, F., Tovar-Sanchez, A., Baudoux, A.-C., and Guieu, C.: N<sub>2</sub> fixation in the Mediterranean Sea related  
 855 to the composition of the diazotrophic community and impact of dust under present and future environmental conditions, *Biogeosciences*, 19, 415–435, <https://doi.org/10.5194/bg-19-415-2022>, 2022.
- Riebesell, U., Reigstad, M., Wassmann, P., Noji, T., and Passow, U.: On the trophic fate of *Phaeocystis pouchetii* (hariot): VI. Significance of *Phaeocystis*-derived mucus for vertical flux, *Netherlands Journal of Sea Research*, 33, 193–203, [https://doi.org/10.1016/0077-7579\(95\)90006-3](https://doi.org/10.1016/0077-7579(95)90006-3), 1995.
- 860 Riegman, R., Noordeloos, A. A. M., and Cad  e, G. C.: *Phaeocystis* blooms and eutrophication of the continental coastal zones of the North Sea, *Marine Biology*, 112, 479–484, <https://doi.org/10.1007/BF00356293>, 1992.
- Robinson, J., Popova, E. E., Srokosz, M. A., and Yool, A.: A tale of three islands: Downstream natural iron fertilization in the Southern Ocean, *Journal of Geophysical Research: Oceans*, 121, 3350–3371, <https://doi.org/10.1002/2015JC011319>, 2016.
- Sarma, V. V. S. S., Yadav, K., and Behera, S.: Role of eddies on organic matter production and f-ratios in the Bay of Bengal,  
 865 *Marine Chemistry*, 210, 13–23, <https://doi.org/10.1016/j.marchem.2019.01.006>, 2019.
- Sarma, V. V. S. S., Chopra, M., Rao, D. N., Priya, M. M. R., Rajula, G. R., Lakshmi, D. S. R., and Rao, V. D.: Role of eddies on controlling total and size-fractionated primary production in the Bay of Bengal, *Continental Shelf Research*, 204, 104186, <https://doi.org/10.1016/j.csr.2020.104186>, 2020.
- Sarma, V. V. S. S., Sridevi, B., Metzl, N., Patra, P. K., Lachkar, Z., Chakraborty, K., Goyet, C., Levy, M., Mehari, M., and  
 870 Chandra, N.: Air-Sea Fluxes of CO<sub>2</sub> in the Indian Ocean Between 1985 and 2018: A Synthesis Based on Observation-Based Surface CO<sub>2</sub>, Hindcast and Atmospheric Inversion Models, *Global Biogeochemical Cycles*, 37, e2023GB007694, <https://doi.org/10.1029/2023GB007694>, 2023.
- Sarmiento, J. L., Gruber, N., Brzezinski, M. A., and Dunne, J. P.: High-latitude controls of thermocline nutrients and low latitude biological productivity, *Nature*, 427, 56–60, <https://doi.org/10.1038/nature02127>, 2004.



- 875 Schlüter, L., Henriksen, P., Nielsen, T. G., and Jakobsen, H. H.: Phytoplankton composition and biomass across the southern Indian Ocean, Deep Sea Research Part I: Oceanographic Research Papers, 58, 546–556, <https://doi.org/10.1016/j.dsr.2011.02.007>, 2011.
- Seeyave, S., Lucas, M. I., Moore, C. M., and Poulton, A. J.: Phytoplankton productivity and community structure in the vicinity of the Crozet Plateau during austral summer 2004/2005, Deep Sea Research Part II: Topical Studies in Oceanography, 54, 2020–2044, <https://doi.org/10.1016/j.dsr2.2007.06.010>, 2007.
- 880 Sherin, C. K., Sarma, V. V. S. S., Rao, G. D., Viswanadham, R., Omand, M. M., and Murty, V. S. N.: New to total primary production ratio (f-ratio) in the Bay of Bengal using isotopic composition of suspended particulate organic carbon and nitrogen, Deep Sea Research Part I: Oceanographic Research Papers, 139, 43–54, <https://doi.org/10.1016/j.dsr.2018.06.002>, 2018.
- Shiomoto, A., Sasaki, H., and Nomura, D.: Size-fractionated phytoplankton biomass and primary production in the eastern Indian sector of the Southern Ocean in the austral summer 2018/2019, Progress in Oceanography, 218, 103119, <https://doi.org/10.1016/j.pocean.2023.103119>, 2023.
- 885 Sieburth, J. McN., Smetacek, V., and Lenz, J.: Pelagic ecosystem structure: Heterotrophic compartments of the plankton and their relationship to plankton size fractions, Limnology and Oceanography, 23, 1256–1263, <https://doi.org/10.4319/lo.1978.23.6.1256>, 1978.
- 890 Tagliabue, A., Sallée, J.-B., Bowie, A. R., Lévy, M., Swart, S., and Boyd, P. W.: Surface-water iron supplies in the Southern Ocean sustained by deep winter mixing, Nature Geosci, 7, 314–320, <https://doi.org/10.1038/ngeo2101>, 2014.
- Takahashi, T., Sutherland, S. C., Wanninkhof, R., Sweeney, C., Feely, R. A., Chipman, D. W., Hales, B., Friederich, G., Chavez, F., Sabine, C., Watson, A., Bakker, D. C. E., Schuster, U., Metzl, N., Yoshikawa-Inoue, H., Ishii, M., Midorikawa, T., Nojiri, Y., Körtzinger, A., Steinhoff, T., Hoppema, M., Olafsson, J., Arnarson, T. S., Tilbrook, B., Johannessen, T., Olsen, A., Bellerby, R., Wong, C. S., Delille, B., Bates, N. R., and de Baar, H. J. W.: Climatological mean and decadal change in surface ocean pCO<sub>2</sub>, and net sea–air CO<sub>2</sub> flux over the global oceans, Deep Sea Research Part II: Topical Studies in Oceanography, 56, 554–577, <https://doi.org/10.1016/j.dsr2.2008.12.009>, 2009.
- 895 Takao, S., Hirawake, T., Wright, S. W., and Suzuki, K.: Variations of net primary productivity and phytoplankton community composition in the Indian sector of the Southern Ocean as estimated from ocean color remote sensing data, Biogeosciences, 9, 3875–3890, <https://doi.org/10.5194/bg-9-3875-2012>, 2012.
- 900 Uitz, J., Claustre, H., Morel, A., and Hooker, S. B.: Vertical distribution of phytoplankton communities in open ocean: An assessment based on surface chlorophyll, Journal of Geophysical Research: Oceans, 111, <https://doi.org/10.1029/2005JC003207>, 2006.
- Uitz, J., Claustre, H., Griffiths, F. B., Ras, J., Garcia, N., and Sandroni, V.: A phytoplankton class-specific primary production model applied to the Kerguelen Islands region (Southern Ocean), Deep Sea Research Part I: Oceanographic Research Papers, 56, 541–560, <https://doi.org/10.1016/j.dsr.2008.11.006>, 2009.



- Uitz, J., Claustre, H., Gentili, B., and Stramski, D.: Phytoplankton class-specific primary production in the world's oceans: Seasonal and interannual variability from satellite observations, *Global Biogeochemical Cycles*, 24, <https://doi.org/10.1029/2009GB003680>, 2010.
- 910 Vaillancourt, R. D., Marra, J., Seki, M. P., Parsons, M. L., and Bidigare, R. R.: Impact of a cyclonic eddy on phytoplankton community structure and photosynthetic competency in the subtropical North Pacific Ocean, *Deep Sea Research Part I: Oceanographic Research Papers*, 50, 829–847, [https://doi.org/10.1016/S0967-0637\(03\)00059-1](https://doi.org/10.1016/S0967-0637(03)00059-1), 2003.
- Vaulot, D., Eikrem, W., Viprey, M., and Moreau, H.: The diversity of small eukaryotic phytoplankton ( $\leq 3 \mu\text{m}$ ) in marine ecosystems, *FEMS Microbiology Reviews*, 32, 795–820, <https://doi.org/10.1111/j.1574-6976.2008.00121.x>, 2008.
- 915 Villareal, T. A., Woods, S., Moore, J. K., and CulverRymza, K.: Vertical migration of *Rhizosolenia* mats and their significance to  $\text{NO}_3^-$  fluxes in the central North Pacific gyre, *Journal of Plankton Research*, 18, 1103–1121, <https://doi.org/10.1093/plankt/18.7.1103>, 1996.
- Wickham H, Averick M, Bryan J, Chang W, McGowan LD, François R, Golemund G, Hayes A, Henry L, Hester J, Kuhn M, Pedersen TL, Miller E, Bache SM, Müller K, Ooms J, Robinson D, Seidel DP, Spinu V, Takahashi K, Vaughan D, Wilke C,
- 920 Woo K, Yutani H (2019). “Welcome to the tidyverse.” *\_Journal of Open Source Software\_*, \*4\*(43), 1686. <https://doi.org/10.21105/joss.01686>
- Wojtasiewicz, B., Trull, T. W., Clementson, L., Davies, D. M., Patten, N. L., Schallenberg, C., and Hardman-Mountford, N. J.: Factors Controlling the Lack of Phytoplankton Biomass in Naturally Iron Fertilized Waters Near Heard and McDonald Islands in the Southern Ocean, *Front. Mar. Sci.*, 6, <https://doi.org/10.3389/fmars.2019.00531>, 2019.
- 925 Zhang, D., Wang, C., Liu, Z., Xu, X., Wang, X., and Zhou, Y.: Spatial and temporal variability and size fractionation of chlorophyll a in the tropical and subtropical Pacific Ocean, *Acta Oceanol. Sin.*, 31, 120–131, <https://doi.org/10.1007/s13131-012-0212-1>, 2012.